Analysis of the Backbone Dynamics of Interleukin-1β Using Two-Dimensional Inverse Detected Heteronuclear ^{15}N–^{1}H NMR Spectroscopy†

G. Marius Clore,*,‡ Paul C. Driscoll,‡ Paul T. Wingfield,§ and Angela M. Gronenborn*,‡

Laboratory of Chemical Physics, Building 2, National Institute of Diabetes and Digestive and Kidney Diseases, National Institutes of Health, Bethesda, Maryland 20892, and Protein Expression Laboratory, Building 6B, National Institutes of Health, Bethesda, Maryland 20892

Received February 28, 1990; Revised Manuscript Received May 1, 1990

ABSTRACT: The backbone dynamics of uniformly ^{15}N-labeled interleukin-1β are investigated by using two-dimensional inverse detected heteronuclear ^{15}N–^{1}H NMR spectroscopy. ^{15}N T_1, T_2, and NOE data at a spectrometer frequency of 600 MHz are obtained for 90% of the backbone amide groups. The data provide evidence for motions on three time scales. All the residues exhibit very fast motions on a time scale of $\lesssim$20–50 ps that can be characterized by a single-order parameter with an average value of 0.82 ± 0.05. For a model comprising free diffusion within a cone, these residue-specific order parameters translate to an average cone semiangle of 20.7 ± 3.3°. Thirty-two residues also display motions on a time scale of 0.5–4 ns, slightly less than the overall rotational correlation time of the protein (8.3 ns). These additional motions must be invoked to account for the discrepancy between experiment and the simplest theoretical formulation in which the internal motions are described by only two parameters, a generalized order parameter and an effective correlation time [Lipari, G., & Szabo, A. (1982a) *J. Am. Chem. Soc. 104*, 4546–4559]. In particular, while the simple formulation can account for the ^{15}N T_1 and T_2 data, it fails to account for the ^{15}N–^{1}H NOE data and yields calculated values for the NOEs that are either too small or negative, whereas the observed NOEs are positive. With the introduction of two internal motions that are faster than the rotational correlation time and differ in time scales by at least 1–2 orders of magnitude [Clore, G. M., Szabo, A., Bax, A., Kay, L. E., Driscoll, P. C., & Gronenborn, A. M. (1990) *J. Am. Chem. Soc. 112*, 4989–4991], all the relaxation data for these 32 residues can be fitted by two order parameters and an effective correlation time for the slower of the two internal motions. A simple model for these two motions is one in which the very fast motion involves axially symmetric diffusion within a cone, while the slower motion comprises jumps between two different orientations of the NH vector. For such a model the jump angle (excluding the C-terminal residue) ranges from 15° to 69° with a mean value of 28.6 ± 14.0°. Another 42 residues are characterized by some sort of motion on the 30-ns–10-ms time scale, which results in ^{15}N line broadening due to chemical exchange between different conformational substates with distinct ^{15}N chemical shifts. In general, the motions on both the 0.5–4-ns and 30-ns–10-ms time scales are localized in surface-accessible loops and turns connecting the β-strands, as well as at the beginning and end of strands. In addition, some of the residues whose ^{15}N line widths are exchange broadened are directly involved in backbone hydrogen bonding with bound internal water molecules or are in close proximity to residues that are. Finally, the kinetic and equilibrium properties of a slow conformational equilibrium between a major and a minor species, involving at least 19 residues and located on one contiguous face of the molecule, are characterized by using ^{1}H–^{15}N correlation spectroscopy, ^{1}H–^{15}N heteronuclear multiple quantum coherence–nuclear Overhauser enhancement spectroscopy, and ^{1}H–^{1}H nuclear Overhauser enhancement spectroscopy.

Protein function is inextricably linked with atomic motion [see, e.g., Careri et al. (1975), Campbell et al. (1978), Debrunner and Frauenfelder (1982), Wodak et al. (1987), and Williams (1989) for reviews]. For example, the recognition process involved in protein–receptor, antigen–antibody, and enzyme–substrate interactions must involve protein flexibility in order to permit both fast recognition and fitting and to enable the appropriate conformational changes required for function to take place (Bennett & Huber, 1983; Ringe & Petsko, 1985; Brooks et al., 1988). Even such simple reactions as the binding of oxygen and carbon monoxide to myoglobin involve a large number of conformational substates (Austin et al., 1975; Ansari et al., 1985). Examples of the types of motion that may occur include local side chain and segmental movements, movement of helices relative to other helices and sheets, hinge movements, and swinging arm motions.

Hormones constitute a classic example of proteins and polypeptides that exert their effects by interacting with other proteins, namely cell surface receptors. One class of hormones is a family of proteins known as cytokines, which play a central role in the immune and inflammatory responses. The topic of the present study is the cytokine interleukin-1β (IL-1β),[1] a protein of 153 amino acids with a molecular mass of 17.4 kDa. The specific activities of IL-1β all involve its interaction

† This work was supported by the Intramural AIDS Targeted Antiviral Program of the Office of the Director of the National Institutes of Health (G.M.C., A.M.G., and P.T.W.).

‡ Laboratory of Chemical Physics.

§ Protein Expression Laboratory.

[1] Abbreviations: IL-1β, interleukin-1β; NMR, nuclear magnetic resonance; T_1, spin–lattice relaxation time; T_2, spin–spin relaxation time; CSA, chemical shift anisotropy; CPMG, Carr–Purcell–Meiboom–Gill; NOE, nuclear Overhauser enhancement; NOESY, two-dimensional nuclear Overhauser enhancement spectroscopy; HMQC, heteronuclear multiple quantum coherence; SD, standard deviation; rms, root mean square.

with a cell surface receptor and include stimulation of B-lymphocyte proliferation, thymocyte proliferation via the induction of interleukin-2 release, prostaglandin and collagenase release, induction of acute-phase protein synthesis by hepatocytes, and fibroblast growth factor activity [see Dinarello (1984, 1988), Oppenheim et al. (1986) and Moore (1989) for reviews]. In two recent papers, we presented the complete resonance assignment of the polypeptide backbone of IL-1β and the determination of its secondary structure and molecular topology, using primarily three-dimensional ^1H–^{15}N heteronuclear NMR spectroscopy (Driscoll et al., 1990a,b). The structural conclusions derived from the NMR data were found to be in complete agreement with two independently solved high-resolution X-ray structures (Finzel et al., 1989; Priestle et al., 1989).

Intramolecular motion can be studied by using a number of experimental and theoretical approaches. Examples of the former include techniques such as NMR spectroscopy [see Jardetzky and Roberts (1981), Wagner (1983), Karplus and Dobson (1986), and Williams (1989) for reviews], fluorescence quenching and lifetime measurements (Lakowicz & Weber, 1973, 1980; Levy & Szabo, 1982; Gratton & Lankowicz, 1985; Bucci & Steiner, 1988; Merola et al., 1989; Bismuto et al., 1989a,b), isotope exchange (Woodward & Hilton, 1979; Englander & Kallenbach, 1983; Wagner, 1983), Mössbauer spectroscopy (Parak et al., 1981, 1982; Bauminger et al., 1983; Parak & Knapp, 1984; Nadler & Schulten, 1984), neutron scattering (Cusack et al., 1988; Dorster et al., 1989) and X-ray crystallography (Frauenfelder et al., 1979; Artymiuk et al., 1979; Hartmann et al., 1982). Theoretical methods generally involve the application of molecular dynamics simulations [see Karplus and McCammon (1981, 1983) and Brooks et al. (1988) for reviews] and normal mode analysis (Brooks & Karplus, 1983; Go et al., 1983; Levitt et al., 1985). Of the various experimental methodologies, only NMR and X-ray crystallography can provide a comprehensive picture of motion of the atomic level. ^{15}N and ^{13}C NMR relaxation measurements provide a powerful means of obtaining such information on fast motions, generally less than the rotational correlation time of the protein (London, 1980; Lipari & Szabo, 1982a,b; Lipari et al., 1982). To date, most of the heteronuclear relaxation data on proteins has been fragmentary and limited by the use of one-dimensional techniques (Allerhand et al., 1971; Glushko et al., 1972; Gust et al., 1975; Hawkes et al., 1975; Norton et al., 1977; Howarth, 1978; London & Avitabile, 1978; Llinas & Wüthrich, 1978; Wittebort et al., 1980; Richarz et al., 1980; Jardetzky et al., 1980; James, 1980; Henry et al., 1986; McCain & Markey, 1987; McCain et al., 1988; Smith et al., 1987; Bogusky et al., 1987; Schiksnis et al., 1987; Dellwo & Wand, 1989). With the advent of new two-dimensional techniques for measuring heteronuclear relaxation (Kay et al., 1989a; Nirmala & Wagner, 1988, 1989), it has now become possible to obtain a detailed and comprehensive picture of these fast motions in proteins.

In this paper we present an analysis of the backbone dynamics of IL-1β using inverse detected ^1H–^{15}N 2D NMR methods. ^{15}N T_1, T_2, and NOE data were obtained for 90% of the backbone amide groups (128 out of a total of 144). We show that all measurable residues exhibit very fast motions on a time scale of $\lesssim$20–50 ps. In addition, 32 residues display a second motion of significant amplitude on a time scale of 0.5–4 ns, which is less than an order of magnitude smaller than the overall rotational correlation time (8.3 ns), while another 42 residues are characterized by an additional motion on the 30-ns–10-ms time scale, which leads to ^{15}N T_2 exchange line broadening. Finally, the kinetic and equilibrium properties of a slow conformational equilibrium between a major and a minor species, involving at least 18 residues, are characterized by using ^1H–^{15}N correlation spectroscopy, ^1H–^{15}N HMQC-NOESY, and ^1H–^1H NOESY.

Experimental Procedures

Sample Preparation. The preparation and purification of des-Ala^1-IL-1β was as described previously (Wingfield et al., 1986; Gronenborn et al., 1986; Driscoll et al., 1990a). This form of IL-1β rather than IL-1β purified from the wild-type gene construct was used, as the latter exhibits N-terminal heterogeneity and comprises a 3:2 mixture of unprocessed and des-Ala^1 forms (Driscoll et al., 1990a,b). Uniform ^{15}N labeling (>95%) was carried out by growing cells in minimal medium containing $^{15}NH_4Cl$ as the sole nitrogen source. Samples for NMR contained ~2 mM protein in 100 mM sodium acetate-d_3 buffer, pH 5.4, in 90% H_2O/10% D_2O.

NMR Spectroscopy. All NMR experiments were carried out at 36 °C on a 600-MHz Bruker AM600 spectrometer operating in "reverse" mode.

The ^1H detected ^{15}N–^1H correlation experiment used a pulse sequence that incorporates a double INEPT transfer of magnetization from ^1H to ^{15}N and back again, known as the "Overbodenhausen" experiment (Bodenhausen & Ruben, 1980; Marion et al., 1989; Bax et al., 1990). The pulse sequence for this experiment is

^1H 90_x–Δ–180_x–Δ–90_y–$t_1/2$–180_x–$t_1/2$–90_x–Δ–180_x–Δ–Acq_χ
^{15}N 180_x $90_{\phi 1}$ $90_{\phi 2}$ 180_x Dec

The delay Δ is set to 2.3 ms, slightly shorter than $1/(4J_{NH})$ to minimize relaxation losses. The pulse in the center of the evolution period for this experiment, as well as in the T_1, T_2, and NOE experiments described below, is a composite 180° ^1H pulse (90_x–180_y–90_x). Time-proportional incrementation (TPPI; Marion & Wüthrich, 1983) is applied to the phase $\phi 1$ to achieve quadrature detection in F_1. The phase cyling employed was as follows: $\phi 1 = x, -x, -x, x$; $\phi 2 = x, x, -x, -x$; and $\chi = x, -x, x, -x$. ^{15}N decoupling in F_2 was carried out by using GARP (Shaka et al., 1985) phase modulation.

The pulse sequences used to measure the ^{15}N T_1 and T_2 relaxation times, as well as the ^1H–^{15}N NOE, have been described in detail by Kay et al. (1989a). They are based on the Overbodenhausen experiment and for the sake of clarity are summarized below.

The sequence used to measure ^{15}N T_1's is

^1H 90_x–Δ–180_x–Δ–$90_{\phi 3}$–τ–180_x–τ–$t_1/2$–180_x–$t_1/2$– –τ–180_x–τ–90_x–Δ–180_x–Δ–Acq_χ
^{15}N 180_x $90_{\phi 2}$ 180_x $90_{\phi 3}$–T–$90_{\phi 4}$ 180_x 90_y 180_x Dec

Quadrature detection is achieved by TPPI of $\phi 3$, and the phase cycling is as follows: $\phi 1 = 8(y), 8(-y)$; $\phi 2 = 4(x), 4(-x)$; $\phi 3 = -y, y$; $\phi 4 = 2(x), 2(-x)$; and $\chi = x, -x, -x, x, -x, x, x, -x, -x, x, x, -x, x, -x, -x, x$. τ is set to $1/(4J_{NH}) = 2.75$ ms. Phase alternation of $\phi 3$ results in the magnetization being stored alternately along the $+z$ and $-z$ axis so that the magnetization relaxes as $\exp(-T/T_1)$. During the relaxation period T, water saturation is also carried out by using off-resonance DANTE pulses. Note that in this pulse sequence, unlike that of Nirmala and Wagner (1988), ^1H decoupling is not used during the interval T. This has *no* influence on the measured T_1's.

The sequence used to measure ^{15}N T_2's is

^1H 90_x–Δ–180_x–Δ–$90_{\phi 1}$–τ–180_x–τ– –180_x– –$t_1/2$–180_x–$t_1/2$–τ–180_x–τ–$90_{\phi 3}$–Δ–180_x–Δ–Acq_χ
^{15}N 180_x $90_{\phi 2}$ 180_x $T/2$ $T/2$ $180_{\phi 4}$ $90_{\phi 5}$ 180_x Dec

A ^{15}N CPMG pulse train $(\delta/2$–$180_{\phi 2}$–$\delta/2)_N$ is applied during the transverse relaxation time T, which minimizes any effects

due to chemical and zero quantum magnetization exchange (i.e., scalar relaxation of the second kind; Ernst et al., 1987). The interval δ between the refocusing pulses in the CPMG train is 1.2 ms. The ^{1}H 180° pulse applied at $T/2$ inverts the water magnetization so that water recovery along the z axis at the end of the period T is negligible. Quadrature in F_1 is achieved by TPPI of $\phi 5$ and the phase cycling is as follows: $\phi 1 = y, -y$; $\phi 2 = 2(x), 2(-x)$; $\phi 3 = 4(x), 4(-x)$; $\phi 4 = 16(x), 16(-x)$; $\phi 5 = 8(x), 8(-x)$; and $\chi = x, -x, -x, x, 2(-x, x, x, -x), x, -x, -x, x$. The $180_{\phi 4}$ pulse is a composite 180° pulse.

The pulse sequence used to record a ^{1}H–^{15}N correlation spectrum with ^{1}H–^{15}N NOE is

$$\begin{array}{lllllllll} ^1\text{H} & \text{sat} & -t_1/2 - 180_x - t_1/2 - \tau - 180_x - \tau - 90_x - \Delta - 180_x - \Delta - \text{Acq}_\chi \\ ^{15}\text{N} & 90_{\phi 1} & & & & 180_x & 90_{\phi 2} & 180_x & \text{Dec} \end{array}$$

^{1}H saturation is achieved by application of 120° pulses spaced at 20-ms intervals for a duration of 3 s prior to the first ^{15}N 90° pulse. During the 20-ms intervals, water suppression is carried out by using an off-resonance DANTE sequence. To record the correlation spectrum without ^{1}H–^{15}N NOE, no ^{1}H saturation is used and water suppression is achieved in a very short period of 100 ms to reduce spin diffusion to the rest of the protein. Quadrature in F_1 is achieved by TPPI of $\phi 1$, and the phase cycling employed is $\phi 1 = x, -x$; $\phi 2 = 2(y), 2(-y)$; and $\chi = x, -x, -x, x$.

All four experiments described above were recorded with a sweep width of 4166.67 Hz in the F_2 dimension with the carrier set to the center of the amide NH region of the spectrum and the water signal on the right-hand edge. Low-power DANTE-style off-resonance irradiation was used to suppress the solvent resonance (Kay et al., 1989b) and, except for the NOE experiments (see above), was applied for 1.7 s. A total of 512 increments, each of 2K data points, were recorded, giving a total acquisition time of 61.44 ms and a sweep width of 2083.3 Hz in the F_1 dimension. Twenty-four transients per t_1 increment were recorded for the T_1 and T_2 experiments, 48 for the NOE experiments, and 32 for the correlation experiment. T_1 values were obtained by using six T delays of 48, 120, 240, 408, 624, and 888 ms, while T_2 values were obtained by using six T delays of 5.36, 26.8, 48.24, 69.68, 96.48, and 117.92 ms.

To examine chemical exchange between major and minor forms of IL-1β, a HMQC-NOESY spectrum (Gronenborn et al., 1989a,b) was recorded with a 50-ms mixing time τ_m. The sequence for this experiment is

$$\begin{array}{llllll} ^1\text{H} & 90_x - \Delta - & & -t_1/2 - 180_{\phi 2} - t_1/2 - & & -\Delta - 90_x - \tau_m - 90_{\phi 4} - \text{Acq}_\chi \\ ^{15}\text{N} & & 90_{\phi 1} & & 90_{\phi 3} & \end{array}$$

The delay Δ is set to 4.5 ms [slightly less than $1/(2J_{NH})$], quadrature in F_1 is obtained by TPPI of $\phi 1$, and the phase cycling is as follows: $\phi 1 = x, -x$; $\phi 2 = 2(x), 2(-x)$; $\phi 3 = 16(x), 16(-x)$; $\phi 4 = 4(x), 4(y), 4(-x), 4(-y)$; and $\chi = 2(x, -x), 2(y, -y), 2(-x, x), 2(-y, y), 2(-x, x), 2(-y, y), 2(x, -x), 2(y, -y)$. This spectrum was recorded with a sweep width of 8333 Hz, with the water resonance in the center of the spectrum. Water suppression was achieved in this case by weak phase-locked coherent irradiation. A total of 256 t_1 increments, each of 128 scans and 2K points, were recorded, giving a total acquisition time of 33.28 ms and a sweep width of 1923 Hz in F_1.

Finally, chemical exchange between major and minor forms of IL-1β was also investigated by means of ^{1}H NOESY (Jeener et al., 1979; Macura et al., 1981) recorded at mixing times of 10, 20, 30, 40, 50, 65, 80, 100, 130, 165, and 200 ms.

Polynomial base-line corrections of order 3 were applied to all the transformed spectra in each dimension. Cross-peak volumes were measured by using the Bruker UXNMR software running on a Bruker X32 computer. In the case of the T_1 and T_2 experiments, the decay of cross-peak intensity with time T was found to be exponential within experimental error. These experimental decays were best fitted to a single exponential by using Powell's method of nonlinear least-squares minimization (Powell, 1965). The time dependence of the chemical exchange peaks in the NOESY spectrum was best fitted by numerical integration of the coupled differential equations describing a two-state model with the program FACSIMILE (Chance et al., 1979; Clore, 1983) operating on a MicroVax III. FACSIMILE employs Curtis' (1979) modified version of Gear's (1967) backward difference method for numerical integration and Powell's (1965) method of optimization, which does not require the computation of partial derivatives. The FACSIMILE program was also used to analyze the ^{15}N relaxation data.

Results

^{15}N T_1, T_2, and NOE Relaxation Data. Figure 1 illustrates a set of three subspectra from the ^{15}N T_1 and T_2 data recorded at 600 MHz. As is evident, the resolution is excellent and we were able to obtain quantitative data for 128 out of a total of 144 backbone amide groups (i.e., 90%). Analysis of the remaining 16 backbone amide groups was precluded due to cross-peak overlap. Figure 2 illustrates the time dependence of the intensities of selected residues covering the full range of ^{15}N T_1 and T_2 values, together with best-fit curves for single-exponential decays. The decay in intensity for all residues was found to be strictly exponential for both the ^{15}N T_1 and T_2 data, and the standard deviations of the best-fit values were all less than 5%, and in the majority of cases less than 2% for the ^{15}N T_1 data. The ^{1}H–^{15}N NOE correlation spectrum is shown in Figure 3. Of greatest interest is that there is only a single residue, namely Ser-153, with a negative NOE. The ^{15}N T_1, T_2, and NOE values are plotted as a function of residue number in Figure 4, and their values and errors are included in the supplementary material.

The T_1 and T_2 relaxation times and the NOE enhancement of an amide ^{15}N spin relaxed by dipolar coupling to a directly bonded proton and by chemical shift anisotropy are given by (Abragam, 1961)

$$1/T_1 = d^2[J(\omega_H - \omega_N) + 3J(\omega_N) + 6J(\omega_H + \omega_N)] + c^2J(\omega_N) \quad (1)$$

$$1/T_2 = 0.5d^2[4J(0) + J(\omega_H - \omega_N) + 3J(\omega_N) + 6J(\omega_H) + 6J(\omega_H + \omega_N)] + c^2[3J(\omega_N) + 4J(0)]/6 \quad (2)$$

$$\text{NOE} = 1 + T_1(\gamma_H/\gamma_N)d^2[6J(\omega_H + \omega_N) - J(\omega_H - \omega_N)] \quad (3)$$

where

$$d^2 = 0.1\gamma_H^2\gamma_N^2\hbar^2\langle r_{HN}^{-3}\rangle^2 \quad (4)$$

and

$$c^2 = (2/15)\omega_N^2(\sigma_\parallel - \sigma_\perp) \quad (5)$$

$\hbar$ is Planck's constant divided by 2π (1.054494×10^{-27} erg·s); γ_H and γ_N are the gyromagnetic ratios of ^{1}H and ^{15}N (2.6753×10^4 and -2.71×10^3 rad·s^{-1}·G^{-1}, respectively); ω_H and ω_N are the nuclear ^{1}H and ^{15}N Larmor frequencies ($2\pi \times 600.13 \times 10^6$ and $2\pi \times 60.8 \times 10^6$ Hz, respectively, at a spectrometer frequency of 600 MHz); r_{HN} is the NH bond length (1.02 Å from neutron diffraction; Keiter, 1986); $\sigma_\parallel$ and $\sigma_\perp$ are the

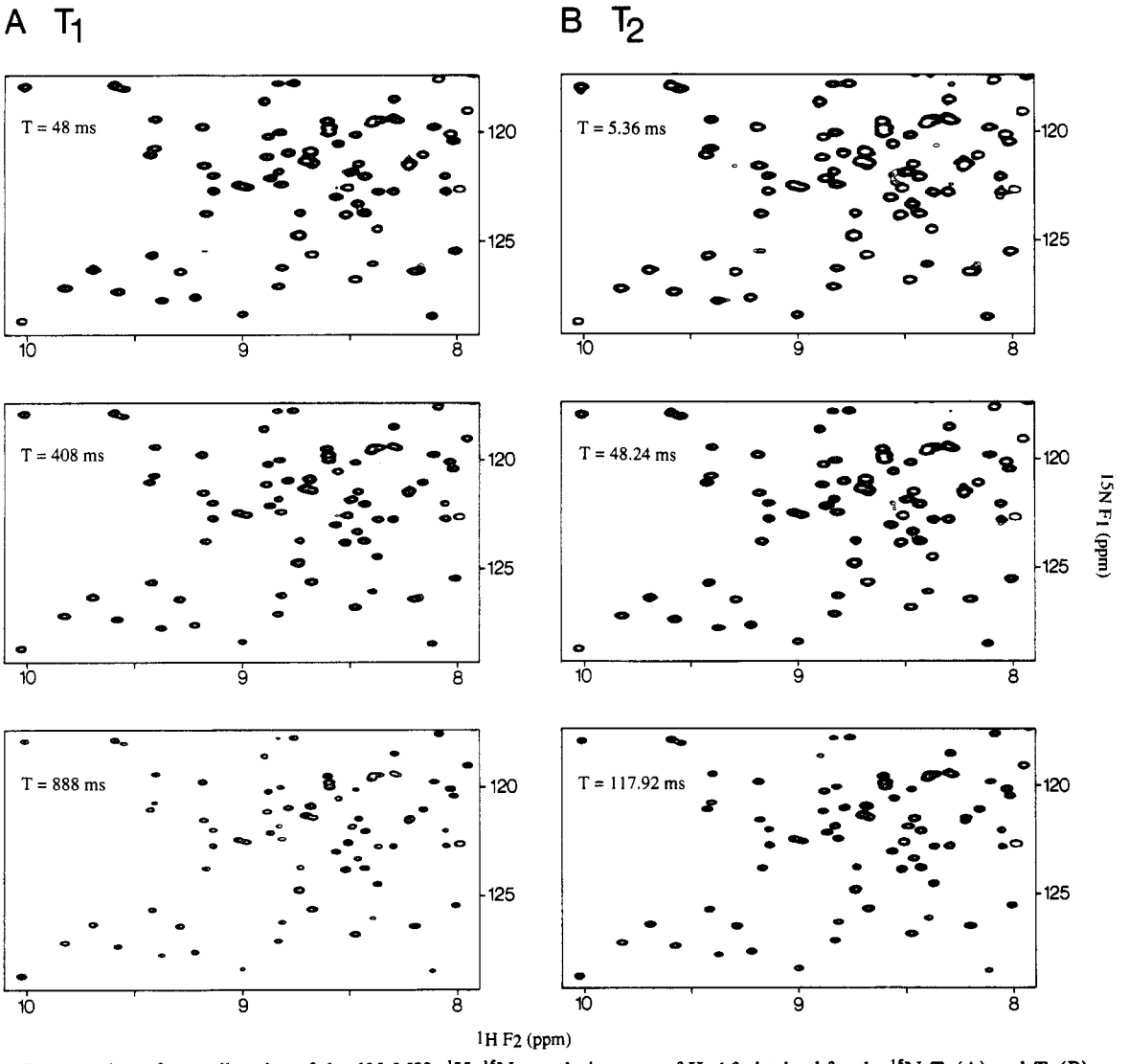

FIGURE 1: Contour plots of a small region of the 600-MHz ^{1}H–^{15}N correlation map of IL-1β obtained for the ^{15}N T_1 (A) and T_2 (B) experiments at different interval times T.

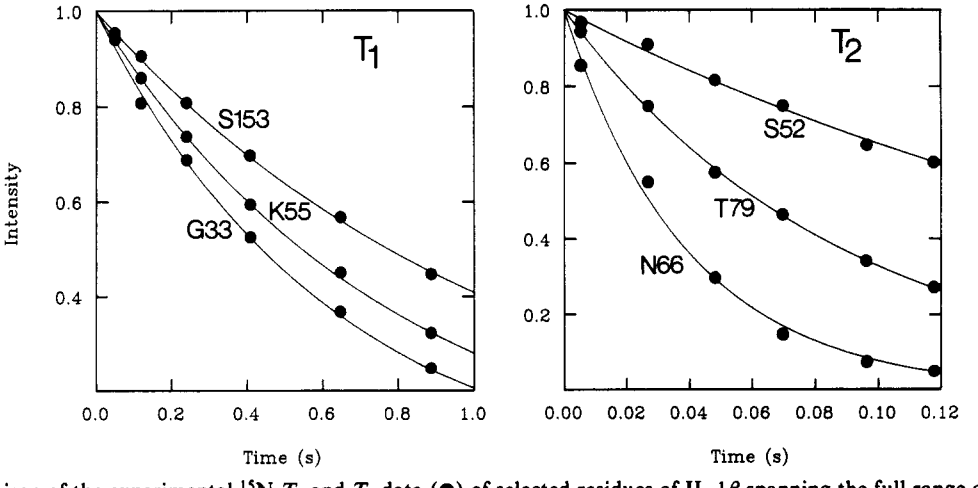

FIGURE 2: Comparison of the experimental ^{15}N T_1 and T_2 data (●) of selected residues of IL-1β spanning the full range of T_1 and T_2 values with the single-exponential least-squares best-fit curves (—).

parallel and perpendicular components of the axially symmetric ^{15}N chemical shift tensor and $(\sigma_\parallel - \sigma_\perp) = -160 \times 10^{-6}$ (Hiyama et al., 1988); and $J(\omega_i)$ is the spectral density function.

In the model-free formalism of Lipari and Szabo (1982a), the internal motions are described by two parameters: a generalized order parameter S and an effective correlation time τ_e. Assuming that the overall and internal motions are independent, the total correlation function $C(t)$ for a macromolecule undergoing isotropic tumbling with a rotational correlation time τ_R is given by

$$C(t) = e^{-t/\tau_R} C_I(t) \quad (6)$$

[Note that, from the X-ray structure of IL-1β (Finzel et al.,

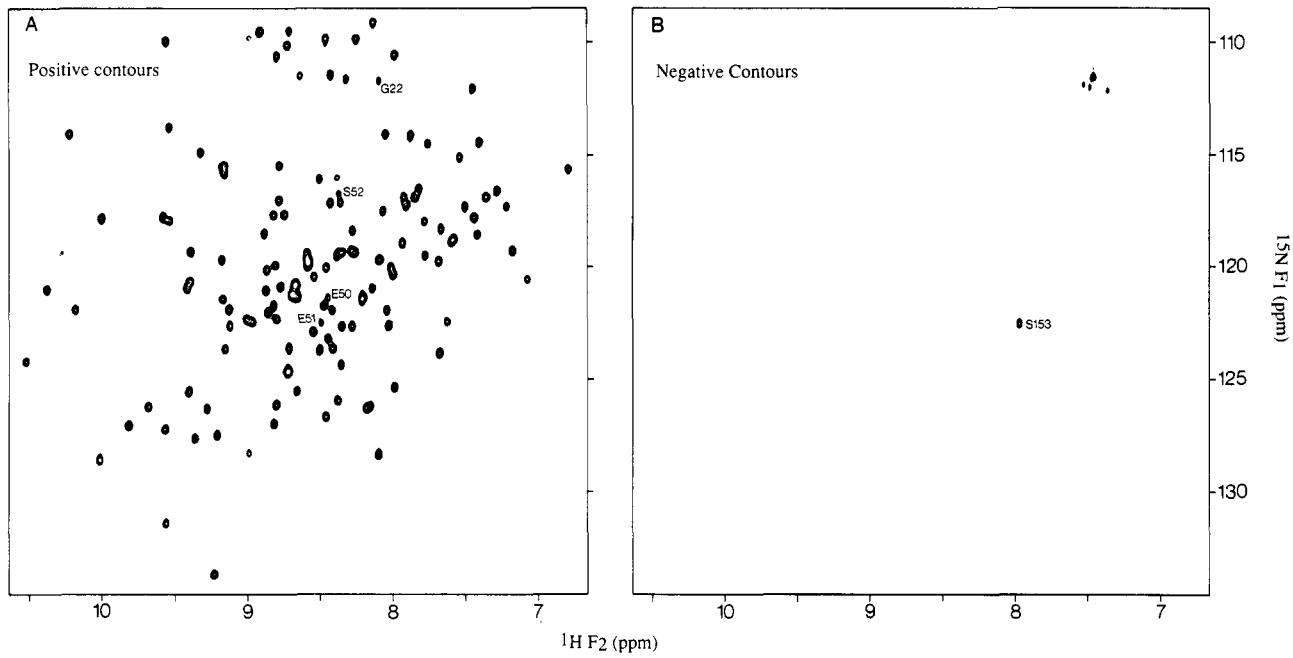

FIGURE 3: Positive- (A) and negative- (B) level contour plots of the 600-MHz ^1H–^{15}N NOE correlation spectrum of IL-1β. The only backbone amide with a negative NOE is Ser-153. The four peaks in the negative contour plot around 112(F_1)/7.5(F_2) ppm arise from side-chain amide protons. Both spectra are plotted on the same contour intensity scale.

1989), the three principal components of the inertia tensor are calculated to be in the ratio of 1.00:0.77:0.93, indicating that IL-1β is a globular, almost spherical, protein that should behave isotropically in solution.] The correlation function $C_I(t)$ for internal motions is in turn given by

$$C_I(t) = S^2 + (1 - S^2)e^{-t/\tau_e} \quad (7)$$

and the corresponding spectral density function has the form

$$J(\omega_i) = S^2\tau_R/(1 + \omega_i^2\tau_R^2) + (1 - S^2)\tau/(1 + \omega_i^2\tau^2) \quad (8)$$

where $\tau = \tau_R\tau_e/(\tau_R + \tau_e)$.

Under conditions where $\tau_e < 100$ ps, $\tau_R > 1$ ns, and T_2 is not significantly shortened by chemical exchange, it is easily shown that the ^{15}N T_1/T_2 ratio is independent of both S and τ_e, allowing a direct determination of the overall rotational correlation time τ_R (Kay et al., 1989a). The mean T_1/T_2 ratio is 8.02 ± 2.68 with a span ranging from 2.61 for Ser-153 to 27.6 for Lys-63. It can be concluded that τ_e makes a significant contribution to T_1 and/or T_2 for those residues with a T_1/T_2 ratio <5.34 (mean minus 1 SD; seven residues, G22, G33, Q34, E50, E51, S52, and S153), while chemical exchange results in a significant shortening of T_2 for those residues with T_1/T_2 >10.7 (mean plus 1 SD; nine residues, K63, E64, K65, N66, L67, D76, V85, I143, and D145). The former are generally manifested by NOE values less than 0.7 and the latter by T_2 values ≲80 ms. As τ_R must clearly be the same for all residues, we excluded from the calculation of τ_R the sixteen residues that had T_1/T_2 ratios outside one standard deviation of the mean. The T_1/T_2 ratios for the remaining 113 residues (mean value of 7.68 ± 0.78) were then fitted *simultaneously* by optimizing a single value of τ_R. This yielded a value of τ_R of 8.3 ± 0.05 ns, which was used in all subsequent analysis. (It should be noted that the rotational correlation time obtained when no residues are excluded is only slightly different, with a value of 8.5 ± 0.15 ns.)

Our approach to the analysis of the relaxation data was to fit the ^{15}N T_1 and T_2 data for each residue *simultaneously*, using a single value of 8.3 ns for the rotational correlation time τ_R, by optimizing the order parameter S^2 and, where appropriate, the effective correlation time for internal motion τ_e or an exchange term to account for chemical exchange contributions to T_2. In the latter case, the observed T_2 is given by

$$1/T_2(\text{obs}) = 1/T_2 + \pi\Delta\text{ex} \quad (9)$$

where T_2 is given by eq 2 and Δex is the increase in line width due to a chemical exchange process.

The ^{15}N T_1 and T_2 data of 54 residues could be fitted by using the simplified spectral density function:

$$J(\omega_i) = S^2\tau_R/(1 + \omega_i^2\tau_R^2) \quad (10)$$

by varying S^2. (A comparison of calculated and observed relaxation data for these residues is given in the supplementary material.) This clearly confirms that IL-1β behaves isotropically in solution and indicates that the internal motions of these residues have small amplitudes ($S^2 > 0.7$) and occur on a time scale ≪100 ps, such that the contribution of the second term of the spectral density function given by eq 8 to T_1 and T_2 is negligible. This is further supported by the observation that all these residues have NOE values of ≳0.7, which puts an upper limit of ~20 ps on the time scale of the internal motions.

In the case of 42 residues that had larger than average ^{15}N T_1/T_2 ratios with concomitantly larger line widths, the ^{15}N T_1 and T_2 data could be fitted by using the simplified spectral density function given by eq 10 in conjunction with an additional chemical exchange term $\pi\Delta\text{ex}$ for T_2 (cf. eq 9). (A comparison of calculated and observed relaxation data for these residues is given in the supplementary material.) It should be noted that the values of S^2 obtained in this manner are the same as those that would be obtained if the T_1 data alone were fitted by using eq 10. Thus, these residues exhibit internal motions on two distinct time scales, one shorter and the other longer than the overall rational correlation time τ_R. Like the 52 residues whose T_1 and T_2 data could be fitted solely by using eq 10, these residues also have NOE values ≳0.7 and are characterized by very fast small amplitude ($S^2 \gtrsim 0.7$) internal motions on a time scale of ≲20 ps. As the time interval between the refocusing pulses of the CPMG sequence used in the T_2 experiment is 1.2 ms, the upper limit for the

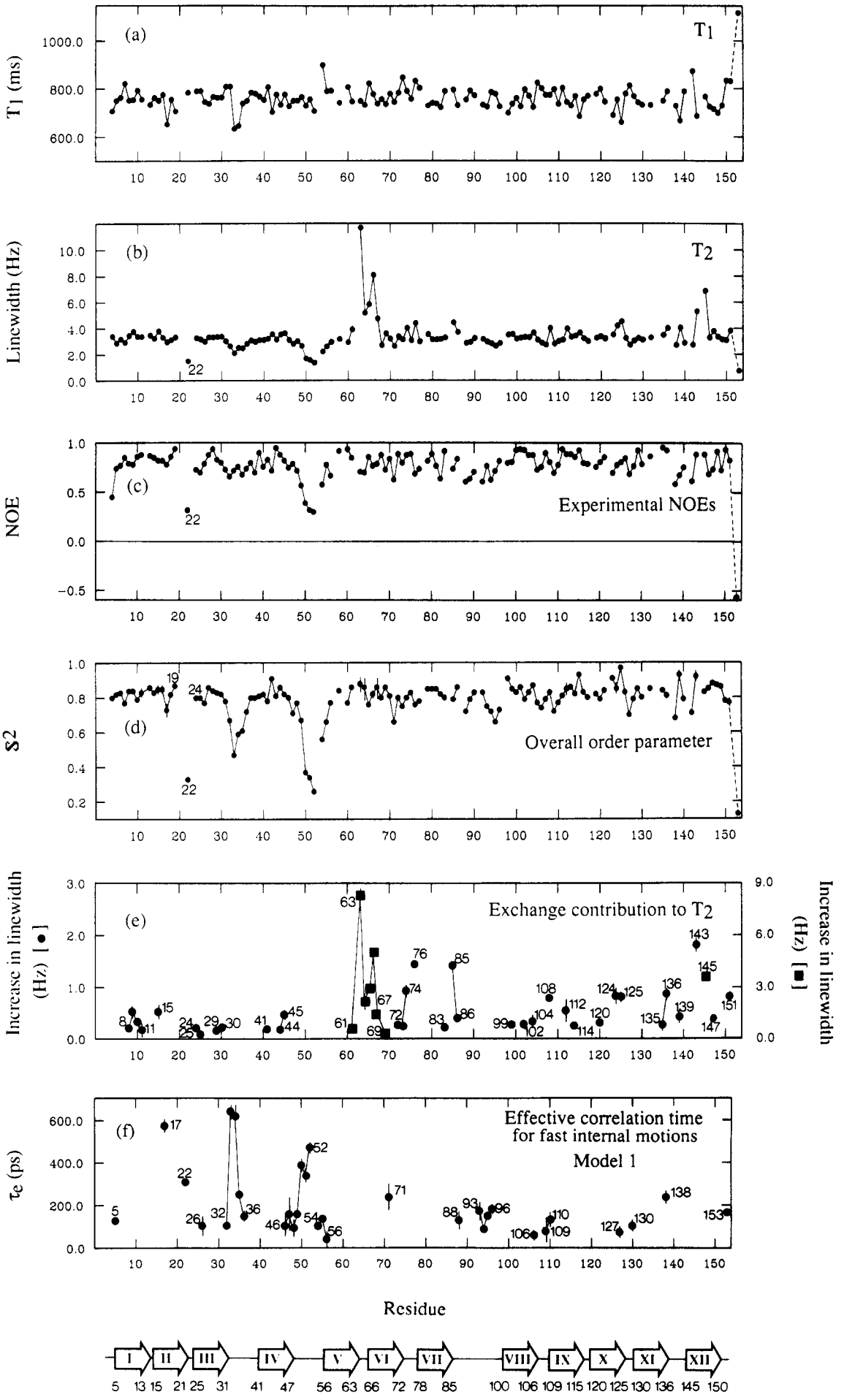
(a)
T1
T1 (ms)
1000.0
800.0
600.0
(b)
T2
Linewidth (Hz)
10.0
8.0
6.0
4.0
2.0
0.0
22
(c)
Experimental NOEs
NOE
1.0
0.5
0.0
−0.5
22
(d)
Overall order parameter
S2
1.0
0.8
0.6
0.4
0.2
19
24
22
(e)
Exchange contribution to T2
Increase in linewidth (Hz) [●]
Increase in linewidth (Hz) [■]
3.0
2.0
1.0
0.0
9.0
6.0
3.0
0.0
63
76
85
74
67
72
61
69
83
86
99
102
104
108
112
114
120
124
125
135
136
139
143
145
147
151
8
11
15
24
25
29
30
41
44
45
(f)
Effective correlation time for fast internal motions
Model 1
τe (ps)
600.0
400.0
200.0
0.0
17
22
5
26
32
36
46
52
54
56
71
88
93
96
106
109
110
127
130
138
153
10 20 30 40 50 60 70 80 90 100 110 120 130 140 150
Residue
I II III IV V VI VII VIII IX X XI XII
5 13 15 21 25 31 41 47 56 63 66 72 78 85 100 106 109 115 120 125 130 136 145 150

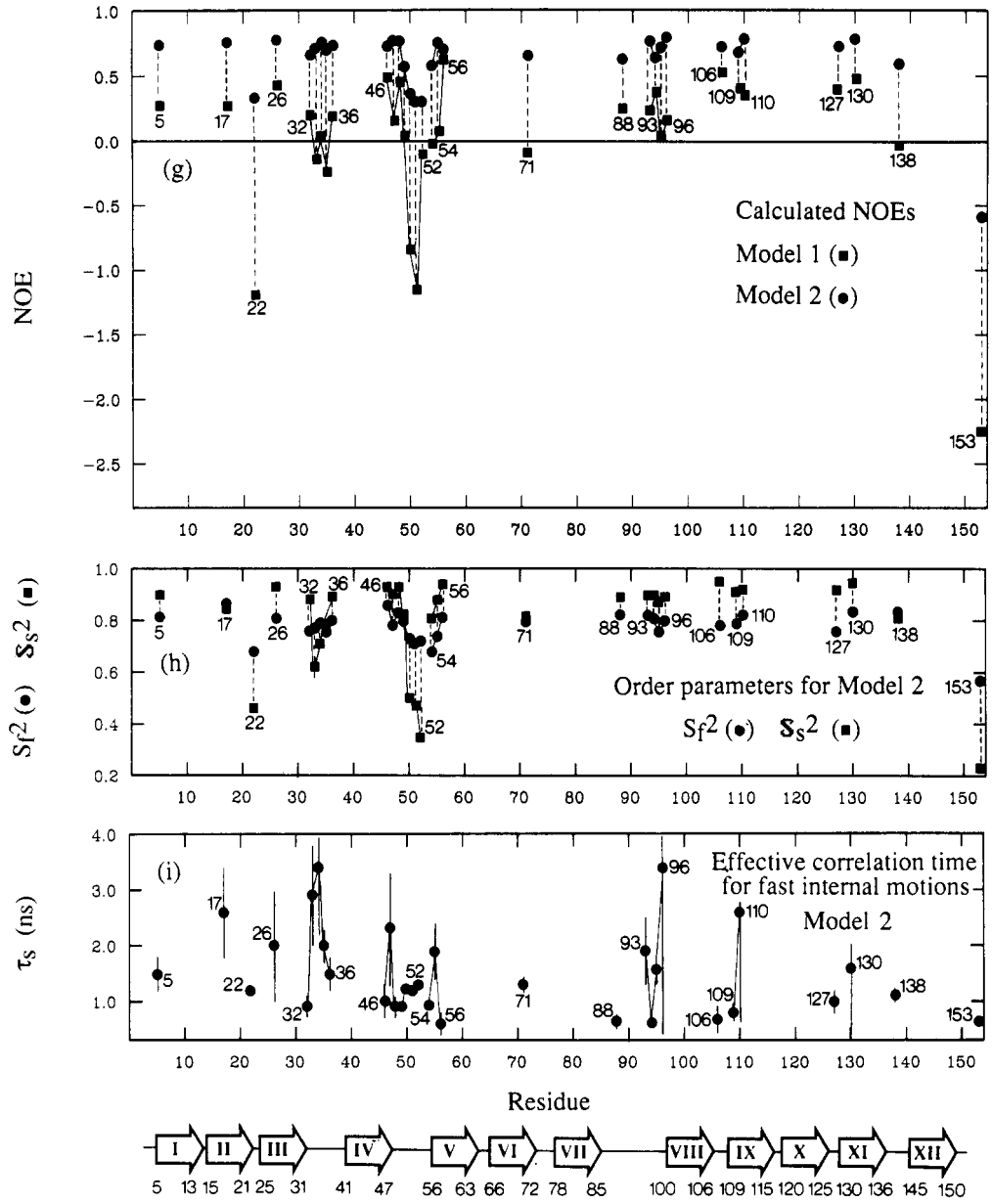

FIGURE 4: Plots as a function of residue number of ^{15}N T_1, T_2 [displayed as line width = $1/(\pi T_2)$] and NOE values measured at 600 MHz, together with various parameters calculated from the data. In the case of 52 of the residues, the relaxation data could be fitted by using the simplified spectral density function given by eq 10. For another 42 residues, the relaxation data could be accounted for by eq 10 in conjunction with eq 9 to account for exchange broadening of ^{15}N line widths. For the remaining 32 residues, the ^{15}N T_1 and T_2 data could be fitted by using the single-internal-motion model (eq 8, referred to as Model 1) but there are large discrepancies between calculated and observed ^1H–^{15}N NOEs (cf. panel c and solid squares in panel g). When a two-internal-motion model (eq 14, referred to as Model 2) is used for these 32 residues, all the experimental relaxation data, including the ^1H–^{15}N NOEs, can be accounted for (cf. panel c and solid circles in panel g). The errors associated with the overall order parameter S^2 are shown as vertical bars. The locations of the 12 β strands, as determined by NMR (Driscoll et al., 1990b), are indicated below the figure.

lifetime of the chemical exchange process is about 10 ms (Kay et al., 1989a). The lower limit depends on the chemical shift difference between the exchanging species. Assuming a maximum ^{15}N chemical shift difference of 10 ppm between two equally populated species and a minimum detectable increase in line width of 0.1 Hz, the minimum value of the exchange lifetime τ_{ex} is calculated to be about 30 ns.

For the remaining 32 residues, the ^{15}N T_1/T_2 ratios are below average and require the use of the full spectral density function given by eq 8 to account for the ^{15}N T_1 and T_2 data. However, while eq 8 can account for the ^{15}N T_1 and T_2 data, it fails to account for the ^1H–^{15}N NOE data. In particular, the calculated values for the NOE are either too small or negative, whereas the observed ones are all positive with the exception of that for Ser-153 (cf. Figures 3 and 4). For example, the calculated NOE values for Gly-22 and Met-138 are −1.2 and −0.02, respectively, whereas the corresponding observed NOEs have values of +0.32 and +0.59, respectively. In this regard, it ought to be pointed out that although the measurement of the NOEs may be subject to small systematic errors and is clearly not as accurate as that of the T_1 and T_2 data, there is no ambiguity in the distinction between positive and negative NOEs. The possible systematic errors in the measurement of the NOEs arise from chemical exchange between water and labile NH protons, which may give rise to an NOE if the recycle time is not sufficiently long relative to the T_1 of water (Smith et al., 1987; Kay et al., 1989a). Given a water T_1 of ~2.5 s for our sample, and a repetition rate of 3 s, approximately 20% of the water is saturated at the start of the experiment recorded without ^1H–^{15}N NOE. For a rapidly exchanging amide proton, the intensity I_{obs} of the ^1H–^{15}N correlation peak in the experiment recorded without

NOE will therefore be reduced relative to its true intensity I by an amount $0.2I(1 - \text{NOE})$. Thus, the effect of rapid NH exchange will be to increase the absolute magnitude of the NOE while preserving its sign: for example, the observed NOE values corresponding to true NOEs of −0.2, 0.2, 0.6, and 0.8 would be −0.26, 0.24, 0.65, and 0.83, respectively. These errors are clearly not sufficient to account for the differences between calculated and observed NOEs, even in those cases where the calculated NOEs are positive. For example, the smallest difference between observed and calculated NOEs is found for Ile-106, where the observed and calculated NOEs have values of 0.76 and 0.52, respectively.

The solution to this apparent discrepancy between the simplest model-free formulation for internal motions and experiment, which has been observed not only in the case of IL-1β but also for a few residues in staphylococcal nuclease, has recently been put forward by Clore et al. (1990). It involves expanding the internal correlation function to a two-exponential decay given by

$$C_I(t) = S^2 + (1 - S_f^2)e^{-t/\tau_f} + (S_f^2 - S^2)e^{-t/\tau_s} \quad (11)$$

The time scales for the two classes of internal motions with correlations times of τ_f and τ_s must differ by at least 1–2 orders of magnitude, otherwise eq 11 effectively approximates to eq 8 as far as the NMR relaxation data are concerned. This is because NMR can only monitor $C_I(t)$ at a few time points at best, and the dissection of closely spaced relaxation processes requires a technique with very high time resolution, such as fluorescence anisotropy decay measurements (Gratton & Lankowicz, 1985). (Of course, the latter suffer from the fact that only very few locations in the molecule can be sampled.) In addition, both internal correlation times must be shorter than the rotational correlation time. S^2 is still the total generalized order parameter for internal motions, while S_f^2 is the generalized order parameter for the faster of the two internal motions. If it is assumed that the fast internal motions are axially symmetric (in which case $S_f^2 = S_f^2$, where S_f is the usual order parameter) and independent of the slow motions, then one can decompose the total generalized order parameter as

$$S^2 = S_f^2 S_s^2 \quad (12)$$

A diagrammatic representation of the time dependence of $C_I(t)$ is shown in Figure 5, which shows that $C_I(t)$ reaches an intermediate value of S_f^2 before finally leveling off at S^2.

The spectral density function corresponding to eqs 11 and 12 is

$$J(\omega_i) = S_f^2 S_s^2 \tau_R/(1 + \omega_i^2 \tau_R^2) + (1 - S_f^2)/(1 + \omega_i^2 \tau_f'^2) + S_f^2(1 - S_s^2)/(1 + \omega_i^2 \tau_s'^2) \quad (13)$$

where $\tau_i' = \tau_i \tau_R/(\tau_R + \tau_i)$, i = f, s. Under conditions where $\tau_f < 10$ ps, eq 13 reduces to

$$J(\omega_i) = S_f^2 S_s^2 \tau_R/(1 + \omega_i^2 \tau_R^2) + S_f^2(1 - S_s^2)/(1 + \omega_i^2 \tau_s'^2) \quad (14)$$

If $S_f^2 = 1$, eqs 13 and 14 reduce to eq 8; if $S_f^2 = S^2$ (i.e., $S_s^2 = 1$), eq 13 reduces to eq 8 and eq 14 to eq 10.

It is clear that we have insufficient data to be able to determine τ_f in eq 13. [It should be noted that collecting data at several spectrometer frequencies would not help in this respect, as the field dependence of T_1 and T_2 can be accounted for by the simple two-parameter internal motion formulation (Clore et al., 1990).] It is therefore instructive to examine the effect of different values of τ_f on the best-fit values obtained for the other three parameters, S_f^2, S_s^2, and τ_s, as well as S^2.

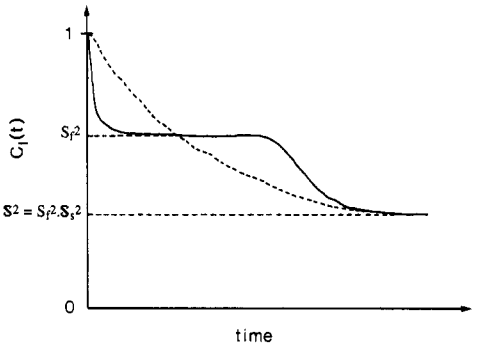

FIGURE 5: Diagrammatic representation of the internal correlation function $C_I(t)$ that can be approximated by a two-exponential decay (eq 11) with lifetimes differing by at least 1 order of magnitude (solid line). Note the plateau at $C_I(t) = S_f^2$. For comparison, the internal correlation function that can be approximated by a single-exponential decay (eq 7) is shown as a dashed line.

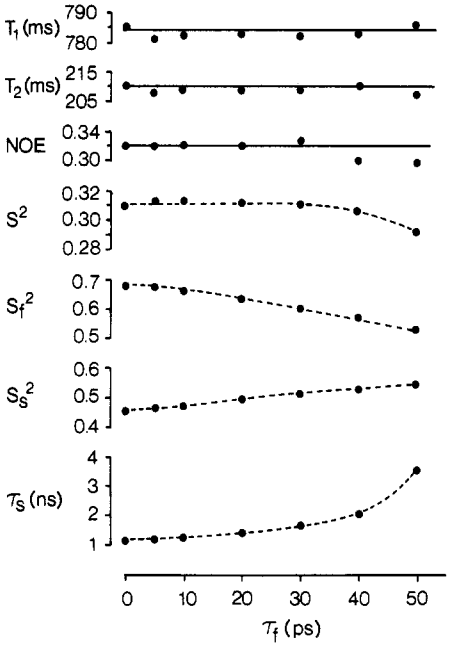

FIGURE 6: Effects of different values of τ_f (from 0 to 50 ps) on the fits and parameters (S_f^2, S_s^2, S^2, and τ_s) obtained by best fitting the ^{15}N T_1, T_2, and NOE data of Gly-22 by using eqs 12 and 13. The experimental T_1, T_2, and NOE values are shown as straight lines and have values of 784 ± 7 ms, 210 ± 11 ms, and 0.32, respectively. Calculated values are shown as solid circles. When τ_f exceeds 50 ps, there is an abrupt phase transition and the experimental data can no longer be fitted.

This is illustrated in Figure 6 for the data on Gly-22. Providing τ_f is less than 50 ps, the T_1, T_2, and NOE data can be fitted by using eq 13. As τ_f is increased from 0 to 50 ps, S_f^2 decreases and S_s^2 and τ_s increase. The product $S_f^2 S_s^2 = S^2$, however, remains constant up to $\tau_f \sim 30$ ps and thereafter decreases. For 30 ps $< \tau_f \lesssim 50$ ps, the relaxation data can still be fitted within the experimental errors of the measurements; however, the calculated values of the NOE are systematically underestimated. As τ_f increases beyond 50 ps, there is an abrupt "phase transition" and the data can no longer be accounted for by eq 13.

To obtain the simplest description consistent with the available data on the 32 anomalous residues, we assumed that τ_f is sufficiently small ($\lesssim$10 ps) so as to make a negligible contribution to the relaxation parameters and proceeded to fit the ^{15}N T_1, T_2, and NOE data *simultaneously* with eq 14 by varying S_f^2, S_s^2, and τ_s. All the relaxation data is fully accounted for and the results are included in Figure 4. (A comparison of the observed relaxation data for these residues

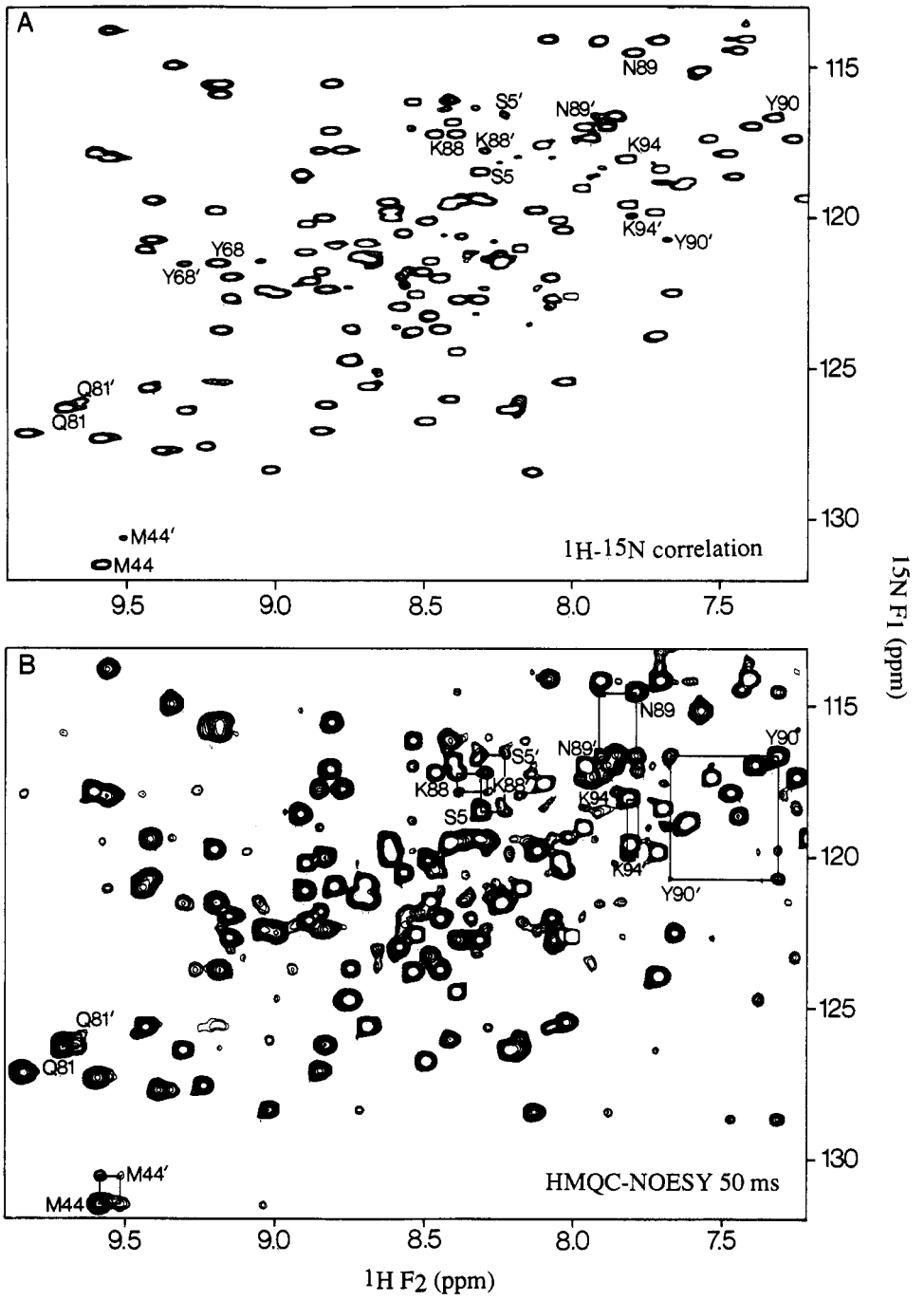

FIGURE 7: Selected region of the Overbodenhausen ^1H–^{15}N correlation (A) and 50-ms ^1H–^{15}N HMQC-NOESY (B) spectra illustrating the presence of a minor species in equilibrium with a major species. The ^1H–^{15}N correlation spectrum yields the equilibrium constant for the process (K_{eq} = 15 ± 1) from the ratios of the peak intensities of the two species, while the rate constants for the exchange process can be extracted from the intensities of the correlation and chemical exchange peaks in the HMQC-NOESY spectrum. The connectivities between the correlation and exchange peaks are indicated by the rectangles with the labels at the position of the correlation peaks.

with the best-fit values obtained by using both eqs 8 and 14 is given in the supplementary material.) It should be noted that the values of the overall order parameter $S^2 = S_f^2 S_s^2$ obtained in this manner are the same as those obtained for the generalized order parameter S^2 when the ^{15}N T_1 and T_2 data alone are fitted by using the single-internal-motion spectral density function given by eq 8. Further, the values of S_f^2 (0.79 ± 0.05) for the anomalous residues are comparable to those of S^2 (0.83 ± 0.05) for the "normal" residues, which lends further support to our assumption that the time scale and physical basis for the faster motion characterizing the 32 anomalous residues is the same as that of the fast internal motion observed for all the other residues. Finally, the computed values of T_1 and T_2 at different spectrometer frequencies are the same from the single- and two-internal-motion formulations, a prediction that has been verified experimentally in the case of staphylococcal nuclease (Clore et al., 1990). Thus, the only difference between the results from eqs 8 and 14 lies in the calculated NOE values.

The effect of the spectral density function given by eq 14 on the calculated NOE values is easily understood by noting that the values of τ_e obtained from fits to the T_1 and T_2 data with eq 8 are approximately an order of magnitude smaller than those for τ_s obtained from fits to the T_1, T_2, and NOE data with eq 14 (see Figure 4). Simulations indicate that, for a τ_R value of 8.3 ns, the NOE reaches a minimum value at an internal correlation time of ~0.25 ns (Clore et al., 1990). Thus, the shift in internal correlation time to larger values that

accompanies the two-internal-motion formulation results in larger values of the NOE while leaving the calculated T_1 and T_2 values unaffected.

It should be noted that, in principle, cases may exist where both T_2 exchange broadening and motions on the 0.5–4-ns time scale coexist in a single residue. Because the former increases the T_1/T_2 ratio, while the latter decreases it, these two effects will compensate each other with regard to the measured relaxation parameters. It is clear that such a case cannot be ascertained from measurements taken at only a single spectrometer frequency, as there are only three measured parameters (T_1, T_2, and NOE) and four unknowns (two order parameters, an effective correlation time for the 0.5–4-ns time scale motion, and an exchange term for the T_2 exchange broadening). In principle, measurements at several spectrometer frequencies may be able to resolve such situations, as the T_1 values will exhibit a much larger frequency dependence than the T_2 values. However, because of the absolute necessity of very high signal-to-noise ratios in order to obtain sufficiently accurate T_1, T_2, and NOE values, the range of spectrometer frequencies amenable for these sorts of experiments is currently limited to the 400–600-MHz range, which is too small a range to be able to discriminate with any degree of confidence between cases with only one of these two processes versus cases where both are present. We have therefore made the simplifying assumption that only one of these two processes can occur for a single residue.

Slow Conformational Exchange between Major and Minor Forms of IL-1β. In our previous paper on the secondary structure of IL-1β (Driscoll et al., 1990b), we noted that a number of residues clustered on one face of the IL-1β structure comprising portions of strands I, IV, V, VI, and VII exhibited conformational heterogeneity between a major and a minor species characterized by an exchange rate that is slow on the NMR chemical shift time scale. We have now extended these observations to the quantification of its equilibrium and kinetic properties. Using the ^1H–^{15}N Overbodenhausen correlation and HMQC-NOESY spectra (Figure 7), we were able to assign the ^{15}N and NH chemical shifts of the major and minor forms for eight residues, namely Ser-5, Met-44, Tyr-68, Gln-81, Lys-88, Asn-89, Tyr-90, and Lys-94. The equilibrium constant obtained from the ratio of the cross-peak intensities in the ^1H–^{15}N correlation spectrum was 15 ± 1. The rate constants for the exchange process were obtained by best fitting the intensities of the correlation peaks and corresponding exchange peaks observed in a single 50-ms HMQC-NOESY experiment (Figure 7) and by fitting the time dependence of the exchange peaks in a series of ^1H–^1H NOESY spectra recorded over a mixing-time range of 10–200 ms (Figure 8) by using the simple two-species model:

$$\xleftarrow{\rho} \mathrm{I} \underset{k_{21}}{\overset{k_{12}}{\rightleftharpoons}} \mathrm{II} \xrightarrow{\rho} \qquad (15)$$

where I and II are the major and minor species, respectively; k_{12} and k_{21} are the rate constants for interconversion between the two species, with an equilibrium constant K given by k_{21}/k_{12}; and ρ is the total spin–lattice relaxation rate of the relevant backbone amide proton, which, for simplicity, is assumed to be the same for the two species. The differential equations describing the time development of magnetization in such a system are given by (McConnell, 1958)

$$\begin{aligned} dM_I/dt &= -M_I(\rho + k_{12}) + k_{21}M_{II} \\ dM_{II}/dt &= -M_{II}(\rho + k_{21}) + k_{12}M_I \end{aligned} \qquad (16)$$

In the case of the 50-ms HMQC-NOESY spectrum, the value of ρ is not critical so it was kept constant at 8 s^{-1}, and only

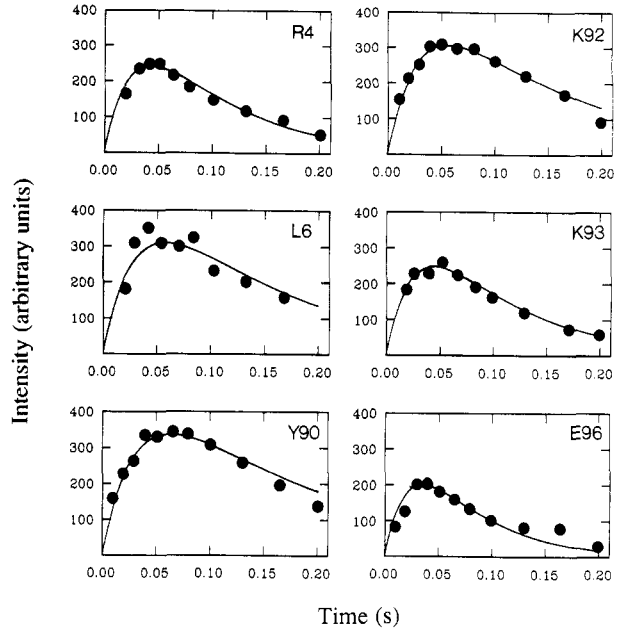

FIGURE 8: Time dependence of the exchange peaks between the major and minor species measured from regular ^1H–^1H NOESY spectra recorded with a series of different mixing times ranging from 10 to 200 ms. The location of the exchange peaks was previously identified in HOHAHA spectra (Driscoll et al., 1990b). The experimental data are represented by solid circles, while the lines represent the best fits obtained by integration of the differential equations give in eq 16. All the data were fitted *simultaneously* by varying the larger of the two rate constants and the individual total spin–lattice relaxation rates, with the equilibrium constant held fixed at the value obtained from the Overbodenhausen ^1H–^{15}N correlation spectrum. The rate constants for the interconversion obtained in this manner are k_{21} = 25 ± 4 s^{-1} and k_{12} = 1.7 ± 0.5 s^{-1}.

k_{21} was varied together with a scale factor (which is proportional to the intensity of the major correlation peak at t = 0). We were only able to measure the intensities of both the major and minor correlation peaks and the exchange peaks for Ser-5, Met-44, and Lys-88. These data yielded a value of k_{21} of 25 ± 4 s^{-1} and a corresponding k_{12} value of 1.7 ± 0.5 s^{-1}. In the case of the NOESY data, we were able to measure the time dependence of the exchange cross-peaks for six other residues, Arg-4, Leu-6, Tyr-90, Lys-92, Lys-93, and Glu-96. Accurate measurement of the intensities of other exchange cross-peaks was precluded due to very small differences in NH chemical shifts between the major and minor forms. The time dependences of all these exchange cross-peaks were fitted *simultaneously* by optimizing the value of k_{21}, a single scale factor (which is proportional to the intensity of the individual diagonal peaks at t = 0 and is assumed to be the same for all residues), and the values of ρ for each residue. The value of k_{21} obtained in this manner was 23 ± 5 s^{-1} with a corresponding k_{12} value of 1.5 ± 0.5 s^{-1}, and the values of ρ ranged from 6.7 s^{-1} for Tyr-90 to 16.7 s^{-1} for Glu-96 (Figure 8). Thus, the data from the HMQC-NOESY and NOESY experiments are in agreement, and the observation that the data for the nine residues can be fitted by using the same equilibrum and kinetic constants strongly suggests that a single common process is involved.

Discussion

We have demonstrated the existence of dynamic processes occuring over four distict time ranges. There are motions that occur on time scales less than 20–50 ps, motions in the range 0.5–4 ns, motions involving species with distinct chemical shifts that can potentially occur over a time range from 30 ns to 10 ms, and finally there is a slow conformational process between

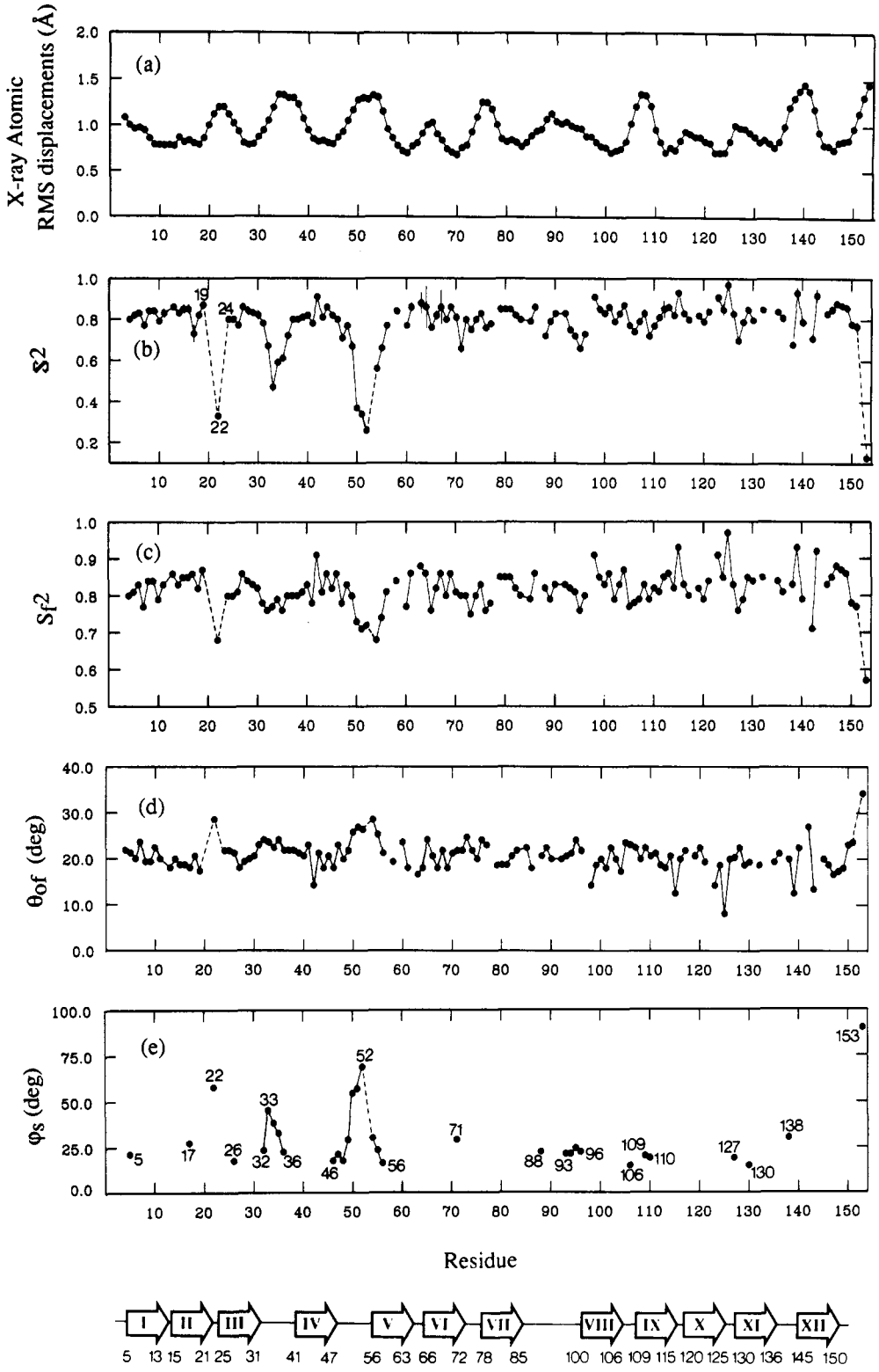

FIGURE 9: Comparison of the backbone nitrogen atomic rms mean displacements derived from X-ray crystallography (Finzel et al., 1989) with the generalized order parameter S^2, the order parameter S_f^2 for motions on a time scale of $\lesssim$20–50 ps, the semiangle θ_{of} for diffusion within a cone derived from S_f^2 by using eq 17, and the jump angle φ_s derived from S_s^2 by using eq 22 for the motions on the 0.5–4-ns time scale. Note that S^2 and S_f^2 are plotted on different scales and with the *exception* of the 32 residues that exhibit two distinct internal motions on a time scale shorter than the rotational correlation time, $S_f^2 = S^2$. The locations of the 12 β strands, as determined by NMR (Driscoll et al., 1990b), are indicated below the figure.

a major and a minor species. We discuss each of these processes in turn.

Very Fast Motions ≲20–50 ps. All the residues exhibit very fast internal motions on a time scale <20–50 ps, and the variation in the order parameter S_f^2 for this motion is depicted in Figure 9. For those residues whose ^{15}N T_1 and T_2 data can be fitted by the simplified spectral density function given by eq 10, the generalized order parameter S^2 is equivalent to the order parameter S_f^2 in the complex spectral density function given by eq 14 with $S_s^2 = 1$. For the 32 anomalous residues that exhibit two distinct internal motions with effective correlation times shorter than the rotational correlation time, the values of S_f^2 are calculated on the assumption that $\tau_f \lesssim$ 10 ps. This seems perfectly reasonable, as the magnitude and

physical basis for the very fast internal motions are likely to be similar for all residues. Indeed, the effective correlation time for those residues whose T_1 and T_2 data can be fitted by using eq 10 must be less than 20 ps to account for their observed NOEs, which have values $\gtrsim 0.7$. Second, the values of S_f^2 for the anomalous residues are comparable to those of S^2 for the remaining residues. If τ_f were larger than 10 ps, S_f^2 would be significantly smaller (cf. Figure 6).

The mean value of S_f^2 is 0.816 ± 0.052, with 5% and 95% confidence limits of 0.712 and 0.920, respectively. Four residues (Ala-115, Ser-125, Gly-139, and Ile-143) have values of S_f^2 above the 95% confidence limits, and all but one of these (Gly-139) are involved in backbone NH---O hydrogen bonds associated with slowly exchanging NH protons (Driscoll et al., 1990b). Four residues (Gly-22, Glu-51, Asp-54, and Ser-153) have S_f^2 values below the 5% confidence limits. Gly-22 is located in a turn between strands II and III, Glu-51 and Asp-54 are in a long loop connecting strands IV and V, and Ser-153 is at the C-terminus. In addition, these four residues are associated with a slower motion on the 0.5–4-ns time scale (see below). It should be noted, however, that the 28 other residues that also exhibit motions on the 0.5–4-ns time scale do not possess unusually small or large values of S_f^2.

Overall, there is little correlation of the variations in exchange kinetics of protected hydrogen-bonded amide protons (Driscoll et al., 1990b) with the measured S_f^2 values. This is perhaps not very surprising, as the dynamic processes leading to amide exchange probably occur on a much slower time scale.

The simplest model for the very fast motions is free diffusion within a cone of semiangle θ_{of}. In this case, the order parameter S_f^2 is simply given by (Lipari & Szabo, 1980, 1981)

$$S_f^2 = [0.5 \cos \theta_{of} (1 + \cos \theta_{of})]^2 \quad (17)$$

The mean value of θ_{of} is 20.7 ± 3.3°, and a plot of θ_{of} as a function of residue is given in Figure 9.

An alternative, but approximately equivalent, representation is to consider that variations in S_f^2 arise from variations in effective bond length r_{eff}. The physical equivalence arises from the fact that the effective bond length depends not only on harmonic and anharmonic vibrations but also on librations (bond bending), such that the trajectory of the NH vector arising from these motions essentially constitutes diffusion within a cone (Lipari & Szabo, 1980). For the case of dipole–dipole interactions with the coordinate system chosen such that the equilibrium bond vector lies along the z axis, it is readily shown that (Henry & Szabo, 1985)

$$r_{eff} \sim R + [\langle \Delta_z \rangle - 2\langle \Delta_z^2 \rangle / R] + \{(\langle \Delta_x^2 \rangle + \langle \Delta_y^2 \rangle)/2R\} \quad (18)$$

where R is the equilibrium internuclear separation (i.e., the distance at the minimum of the potential well), and Δx, Δy, and Δz are the instantaneous displacement vectors in the x, y, and z directions. The term in square brackets arises from the vibrational averaging of the intrinsic coupling constant (i.e. $\langle r^{-3} \rangle^{-1/3}$), while the terms in braces arise from averaging of the orientation of the internuclear vector (i.e., librations). The harmonic vibration term $2\langle \Delta_x^2 \rangle / R$ always tends to reduce r_{eff}, while the anharmonic vibration term Δ_z and the libration (bond bending) terms always tend to increase r_{eff}. From eqs 4, 8, and 14 we obtain

$$S_f^2 \sim (R/r_{eff})^6 \quad (19)$$

The value of R that was used throughout is 1.02 Å and was obtained from neutron diffraction data (Keiter, 1986). Excluding the C-terminal residue Ser-153, r_{eff} would then range from 1.088 Å for Gly-22 and Asp-54 to 1.025 Å for Ser-125, which corresponds to increases in effective bond length of 6.6% and 0.5%, respectively. In the case of Ser-153, the relative increase in effective bond length would be ~9.8%.

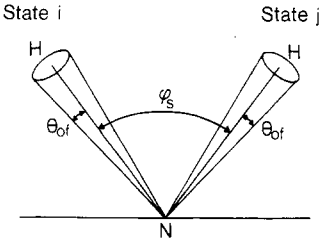

FIGURE 10: Model of the motions for residues with two internal motions on time scales <20–50 ps and 0.5–4 ns. The slower motion is represented by a jump between two states i and j, while the faster motion is represented as free diffusion within two axially symmetric cones centered about the two states i and j. θ_{of} is the semiangle of the cone, while φ_s is the angle between the NH vectors in the two states i and j.

Fast Motions on the 0.5–4-ns Time Scale. The relaxation data for 32 residues can only be accounted for if two internal motions faster than the rotational correlation time τ_R are taken into consideration. One of the motions, discussed above, is very fast, with a time scale that must be less than 50 ps and in all likelihood is less than 10 ps, while the other is at least 1–2 orders of magnitude slower and has a lifetime of 0.5–4 ns. One residue (Ser-153) is located at the C-terminus, 21 are in turns or loops at the surface of the protein, and the remaining 10 are at the very beginning or end of a strand. The amplitudes of these motions are described by S_s^2 in eqs 12 and 14; the largest amplitudes are found in the turn connecting strands II and III (Gly-22) and in the loops connecting strands III and IV (Gln-32–Met-36) and strands IV and V (Phe-46–Ile-56).

A simple model for these motions is depicted in Figure 10. We consider that the two motions associated with the order parameters S_f and S_s are totally independent. The very fast motion is assumed to involve axially symmetric diffusion within a cone, while the slower motion is depicted as a two-state jump model. These two motions can be pictured as representing the fast random thermal motions and the rare discrete transitions typically observed in theoretical molecular dynamics simulations (Karplus & McCammon, 1979, 1983; Levitt, 1983; Elber & Karplus, 1987; Brooks et al., 1988; Levitt & Sharon, 1988; Post et al., 1989). Because the two sets of motions are independent, the NH vector, which is located anywhere within the first cone, can jump to any position within the second cone. The exact internal correlation function for this model, which precisely corresponds to the spectral density function given by eq 14, is

$$C_I(t) = S_f^2\{C_s(\infty) + [C_s(0) - C_s(\infty)]e^{-(k_{ij}+k_{ji})t}\} \quad (20)$$

where $C_s(0) = 1$, $C_s(\infty) = S_s^2$, and k_{ij} and k_{ji} are the rate constants for jumps between the two states i and j with $k_{ij} + k_{ji} = 1/\tau_s$. S_s^2 is then given by (Wittebort & Szabo, 1978)

$$S_s^2 = C_s(\infty) = \sum_i \sum_j p_{eq}(i) p_{eq}(j) P_2(\cos \varphi_{ij}) \quad (21)$$

where $p_{eq}(i)$ and $p_{eq}(j)$ are the probabilities for residency in states i and j, with $p_{eq}(i) + p_{eq}(j) = 1$ and $p_{eq}(i)/p_{eq}(j) = k_{ji}/k_{ij}$, and $P_2(\cos \varphi_s)$ is a second-order Legendre polynomial given by $P_2(\cos \varphi_s) = (3 \cos^2 \varphi_s - 1)/2$, where φ_s is the angle between the NH vector in states i and j. For the simplest case where $p_{eq}(i) = p_{eq}(j) = 0.5$, we have

$$S_s^2 = (1 + 3 \cos^2 \varphi_s)/4 \quad (22)$$

with a minimum value of 0.25 when $\varphi_s = 90°$. In the case of Ser-153, the measured value of S_s^2 is very close to 0.25. For the other 31 residues, S_s^2 ranges from 0.35 for Ser-52 to 0.95 for Ile-106 and Met-130, which corresponds to a range of φ_s from 69° to 15°. The mean value of φ_s, excluding Ser-153, is 28.6 ± 14.0°, and a plot of φ_s as a function of residue number is shown in Figure 9.

Motions Causing ^{15}N T_2 Exchange Broadening. There are 42 residues that exhibit some type of motion on a time scale ranging from 30 ns to 10 ms, which causes exchange broadening of the ^{15}N line widths. As these motions must involve at least two species with different chemical shifts, the simplest model is once again a two-state jump model. However, as the chemical shift differences are unknown, no estimation of the rates of these processes can be ascertained. Further, the experimental data afford no information on the magnitude of these motions.

The largest line broadening effects are seen in the turn connecting strands V and VI (residues 63–66) and at the beginning of strand 12 (residue 145). Some residues (72, 73, 74, and 76) in the loop connecting strands VI and VII are also exchange broadened, as are many residues at the beginning and end of strands. One exception to this is seen for strand I, where the central residues (8–11) are exchange broadened.

Examination of the refined high-resolution 2.0-Å X-ray structure (Finzel et al., 1989) of IL-1β reveals the presence of eight tightly bound internal water molecules involved in hydrogen bonding with the backbone amide and carbonyl groups. It is interesting to note that a number of the residues whose ^{15}N resonances are exchange broadened are directly involved in these hydrogen bonds. These include Leu-10, Met-44, Phe-112, Ser-125, and Val-151. Further, a number of other exchange-broadened residues are in close proximity to residues directly involved in hydrogen bonding with water. For example, Ile-143 and Asp-145 are adjacent to Thr-144, Cys-8 and Ser-45 are adjacent to Asn-7 and Met-44, respectively, and Val-41 is close to Ser-43. Thus, the exchange line broadening seen for these ^{15}N resonances most likely arises from exchanging bound water molecules that are involved in secondary structure stabilization, such as bridging backbone hydrogen bonds.

Slow Conformational Heterogeneity between a Major and a Minor Species. From the data presented in this paper as well as the previous paper (Driscoll et al., 1990b), we have been able to identify a total of 19 residues that exist in two interchanging conformations, comprising a major and a minor species. These are Val-3, Arg-4, Ser-5, Leu-6, Met-44, Phe-46, Gly-49, Glu-50, Tyr-68, Gln-81, Leu-82, Val-85, Asp-86, Lys-88, Asn-89, Tyr-90, Lys-92, Lys-93, and Glu-96. We have been able to characterize the equilibrium and/or kinetic properties of the exchange process for 13 of these and have found them to be identical within the errors of the data, suggesting that a single common process is involved. This process is superimposed on other motional characteristics. Thus, four of these residues (44, 68, 85, and 86) also exhibit some sort of motion on the 30-ns–10-ms time scale, which results in broadening of ^{15}N line widths, while seven of the residues (5, 46, 49, 50, 88, 93, and 96) exhibit two distinct motions that are faster than the rotational correlation time.

All of the above residues are located in one distinct region of the molecule, at the corner of the approximately tetrahedral protein structure where the loop (residues 86–88) connecting strands VII and VIII meets the N-terminus. This loop is considerably longer (14 amino acids) than the equivalent ones at the junction of either strands III and IV (9 amino acids) or strands XI and XII (8 amino acids) in the three pseudosymmetric βββLβ units (Finzel et al., 1989; Driscoll et al., 1990b) that make up the protein, thereby allowing a larger degree of conformational flexibility for this segment of polypeptide chain. This possible conformational freedom, in conjunction with the fact that the β-sheet structure in this corner involves the N-terminal strand, could well account for the two distinct conformations observed for this part of the protein. The precise origin of these two conformations is not clearly established at the present time. The possibility of a cis–trans isomerization involving Pro-91 can be ruled out because the interconversion rates between the two species are 2 orders of magnitude faster than the highest rates observed for cis–trans proline isomerization (Evans et al., 1989). Thus, it seems more likely that two conformational species arise from slightly different arrangements of the 86–99 loop.

Correlation with Crystallographic B-Factors. There has been considerable interest in the literature in using crystallographic *B*-factors to analyze intramolecular motion in proteins and correlate it with function (Frauenfelder et al., 1979; Artymiuk et al., 1979; Sternberg et al., 1979; Hartmann et al., 1982; Westhof et al., 1984; Tainer et al., 1984). The Debye–Waller *B*-factors provide a measure of the mean square displacement of the atoms in the crystal through the relationship $\langle x^2 \rangle = (3B/8\pi^2)^{1/2}$ (Willis & Pryor, 1975), and a plot of the rms atomic displacements for the backbone nitrogen atoms of IL-1β is shown in Figure 9. The X-ray data, however, provide no information on the time scale of the motions. Further, deconvolution of the *B*-factor into its individual components comprising vibrations, conformational fluctuations, and lattice disorder is difficult. Nevertheless, it is instructrive to compare the X-ray and NMR data.

In addition to the N- and C-termini, the X-ray data reveal 10 regions in the polypeptide backbone with unusually large atomic rms displacements, which are located in the turns and loops connecting the β-strands (Figure 9). In general, these are correlated with either the presence of motion on the 0.5–4-ns time scale superimposed on a very fast motion (time scale ≲20–50 ps) or by motion on the 30-ns–10-ms time scale. The high *B*-factors in the turn connecting strands II and III, and in the loops connecting strands III and IV, and strands IV and V are thus correlated with unusually low values of the generalized order parameter S^2 and the presence of large-scale amplitude motion on the 0.5–4-ns time scale, manifested by low values of S_s^2 and concomitant large jump angles φ_s (Figure 9). Likewise, the high *B*-factors in the loops connecting strands VII and VIII, VIII and IX, X and XI, and XI and XII are associated with the presence of residues exhibiting smaller scale amplitude motions on the 0.5–4-ns time scale. The two regions where motions on the 30-ns–10-ms time scale result in the largest increases in T_2 line width, namely in the regions connecting strands V and VI (residues 61–69) and strands IX and XII (residues 135–147), are also correlated with large *B*-factors (cf. Figures 4 and 9). However, not all those residues that are exchange broadened are associated with above average *B*-values. For example, residues 8–11, 15, 29, 30, 41, 44, 45, 83, 99, 102, 112, 124, 125, 135, 136, 145, and 147 all display increases in ^{15}N line widths due to an exchange contribution to T_2, and yet they exhibit among the smallest backbone atomic rms displacements in the crystal structure, being located in the troughs of the *B*-factor curve.

The lack of perfect correlation between the NMR and crystal data on atomic mobility is not surprising and may be due to a number of factors. First, motion that does not result in reorientation of the NH vector with regard to the magnetic field will not be manifested in the ^{15}N NMR relaxation data. Second, some motion in the crystal may be reduced as a result

of crystal contacts. Thus the turns connecting strands I and II, V and VI, IX and X, and X and XI, as well as the loop joining strands VII and VIII, are all involved in contacts with adjoining molecules in the crystal lattice and exhibit *B*-values somewhat lower than the other turns and loops that are not involved in such contacts. In contrast, the largest effects on T_2 line broadening are associated with the turn connecting strands V and VI. Third, some regions that are mobile in solution and sample a range of conformations may be locked in a single conformational state upon crystallization.

Concluding Remarks. In conclusion, the picture of protein backbone motion that we obtain from the present study is one in which very fast motions occur throughout the protein and are superimposed in certain regions on slower motions. The fast motions probably represent local oscillations. The slow ones, which can occur on widely ranging time scales from nanoseconds to milliseconds, arise from transitions between different conformational substates and are generally located in surface-exposed turns and loops.

ACKNOWLEDGMENTS

We thank Dr. Attila Szabo for numerous stimulating and enlightening discussions and for critically reading the manuscript. We also thank Drs. Ad Bax and Lewis Kay for useful discussions.

SUPPLEMENTARY MATERIAL AVAILABLE

One table giving the values and errors of the experimental ^{15}N T_1, T_2, and NOE relaxation data together with the best-fit values for the calculated relaxation data and the optimized values of the order parameters, effective correlation times, and T_2 line broadening parameters (24 pages). Ordering information is given on any current masthead page.

REFERENCES

Abragham, A. (1961) *The Principles of Nuclear Magnetism*, Clarendon Press, Oxford, England.

Allerhand, A., Doddrell, D., Glushko, V., Cochran, D. W., Wenkert, E., Lawson, P. J., & Gurd, F. R. N. (1971) *J. Am. Chem. Soc. 93*, 544–546.

Ansari, A., Berendsen, J., Bowne, S. F., Frauenfelder, H., Iben, I. T. E., Sauke, T. B., Shyamsunder, E., & Young, R. D. (1985) *Proc. Natl. Acad. Sci. U.S.A. 82*, 5000–5004.

Artymiuk, P. J., Blake, C. C. F., Grace, D. E. P., Oatley, S. J., Philips, D. C., & Sternberg, M. J. E. (1979) *Nature 280*, 563–568.

Austin, R. H., Beeson, K. W., Eisenstein, L., Frauenfelder, H., & Gunsalus, I. C. (1975) *Biochemistry 14*, 5355–5373.

Bax, A., Ikura, M., Kay, L. E., Torchia, D. A., & Tschudin, R. (1990) *J. Magn. Reson. 86*, 304–318.

Bauminger, E. R., Cohen, S. G., Nowik, I., Ofer, S., & Yariv, J. (1983) *Proc. Natl. Acad. Sci. U.S.A. 80*, 736–740.

Bennett, W. S., & Huber, R. (1983) *CRC Crit. Rev. Biochem. 15*, 291–384.

Bismuto, E., Irace, G., & Gratton, E. (1989a) *Biochemistry 28*, 1508–1512.

Bismuto, E., Sirangelo, I., & Irace, G. (1989b) *Biochemistry 28*, 7542–7545.

Bodenhausen, G., & Ruben, D. J. (1980) *Chem. Phys. Lett. 69*, 185–189.

Bogusky, M. J., Schiksnis, R. A., Leo, G. C., & Opella, S. J. (1987) *J. Magn. Reson. 72*, 186–190.

Brooks, B. R., & Karplus, M. (1983) *Proc. Natl. Acad. Sci. U.S.A. 80*, 6571–6575.

Brooks, C. L., Karplus, M., & Pettitt, B. M. (1988) *Adv. Chem. Phys. 71*, 1–259.

Bucci, E., & Steiner, R. F. (1988) *Biophys. Chem. 30*, 199–224.

Campbell, I. D., Dobson, C. M., & Williams, R. J. P. (1978) *Adv. Chem. Phys. 39*, 55–107.

Careri, G., Fasella, P., & Gratton, E. (1975) *CRC Crit. Rev. Biochem. 3*, 141–164.

Chance, E. M., Curtis, A. R., Jones, I. P., & Kirby, C. R. (1979) *U.K. At. Energy Auth., Harwell Lab., [Rep.] AERE-R 8775.*

Clore, G. M. (1983) in *Computing in Biological Science* (Geisow, M. J., & Barrett, M., Eds) pp 313–348, Elsevier North-Holland, Amsterdam, The Netherlands.

Clore, G. M., Szabo, A., Bax, A., Kay, L. E., Driscoll, P. C., & Gronenborn, A. M. (1990) *J. Am. Chem. Soc. 112*, 4989–4991.

Curtis, A. R. (1979) *U.K. At. Energy Auth., Harwell Lab., [Rep.] AERE-R 9352.*

Cusack, S., Smith, J., Finney, J., Tidor, B., & Karplus M. (1988) *J. Mol. Biol. 202*, 903–908.

Debrunner, P. G., & Frauenfelder, H. (1982) *Annu. Rev. Phys. Chem. 33*, 283–299.

Dellwo, M. J., & Wand, A. J. (1989) *J. Am. Chem. Soc. 111*, 4571–4578.

Dinarello, C. A. (1984) *Rev. Infect. Dis. 6*, 51–95.

Dinarello, C. A. (1988) *Ann. N.Y. Acad. Sci. 546*, 122–132.

Dorster, W., Cusack, S., & Petry, W. (1989) *Nature 337*, 754–756.

Driscoll, P. C., Clore, G. M., Marion, D., Wingfield, P. T., & Gronenborn, A. M. (1990a) *Biochemistry 29*, 3542–3556.

Driscoll, P. C., Gronenborn, A. M., Wingfield, P. T., & Clore, G. M. (1990b) *Biochemistry 29*, 4668–4682.

Elber, G., & Karplus, M. (1987) *Science 235*, 318–321.

Englander, S. W., & Kallenbach, N. R. (1984) *Q. Rev. Biophys. 16*, 521–655.

Ernst, R. R., Bodenhausen, G., & Wokaun, A. (1987) *Principles of Nuclear Magnetic Resonance in One and Two Dimensions*, Oxford University Press, Oxford, England.

Evans, P. A., Kautz, R. A., Fox, R. O., & Dobson, C. M. (1989) *Biochemistry 28*, 362–370.

Finzel, B. C., Clancy, L. L., Holland, D. R., Muchmore, S. W., Watenpaugh, K. D., & Einspahr, H. M. (1989) *J. Mol. Biol. 209*, 779–791.

Frauenfelder, H., & Petsko, G. A. (1980) *Biophys. J. 32*, 465–478.

Frauenfelder, H., Petsko, G. A., & Tsernoglou, D. (1979) *Nature 280*, 558–562.

Gear, C. W. (1967) *Math. Comp. 21*, 146–156.

Glushko, V., Lawson, P. J., & Gurd, F. R. N. (1972) *J. Biol. Chem. 247*, 3176.

Go, N., Noguti, T., & Nishikawa, T. (1983) *Proc. Natl. Acad. Sci. U.S.A. 80*, 3696–3700.

Gratton, E., & Lankowicz, J. R. (1985) in *Structure and Motion: Membranes, Nucleic Acids and Proteins* (Clementi, E., Corongiu, G., Sarma, M. H., & Sarma, R. H., Eds.) pp 155–168 and 4741–4758, Adenine Press, Guilderland, NY.

Gronenborn, A. M., Wingfield, P. T., Schmeissner, U., & Clore, G. M. (1986) *Eur. J. Biochem. 161*, 37–43.

Gronenborn, A. M., Bax, A., Wingfield, P. T., & Clore, G. M. (1989a) *FEBS Lett. 243*, 93–98.

Gronenborn, A. M., Wingfield, P. T., & Clore, G. M. (1989b) *Biochemistry 28*, 5081–5089.

Gust, D., Moon, R. B., & Roberts, J. D. (1975) *Proc. Natl. Acad. Sci. U.S.A. 72*, 4696–4700.

Hartmann, H., Parak, F., Steigemann, W., Petzko, G. A., & Ringe, D. (1982) *Proc. Natl. Acad. Sci. U.S.A. 79*, 4967–4971.
Hawkes, G. E., Randall, E. W., & Bradley, C. H. (1975) *Nature 257*, 767–772.
Henry, E. R., & Szabo, A. (1985) *J. Chem. Phys. 82*, 4753–4761.
Henry, G. D., Weiner, J. H., & Sykes, B. D. (1986) *Biochemistry 25*, 590–598.
Hiyama, Y., Niu, C., Silverton, J. V., Bavaso, A., & Torchia, D. A. (1988) *J. Am. Chem. Soc. 110*, 2378–2383.
Howarth, O. W. (1978) *J. Chem. Soc., Faraday Trans. 2 74*, 1031–1046.
James, T. L. (1980) *J. Magn. Reson. 39*, 141–153.
Jardetzky, O., & Roberts, G. C. K. (1981) *NMR in Molecular Biology*, Academic Press, New York.
Jardetzky, O., Ribeiro, A. A., & King, R. (1980) *Biochem. Biophys. Res. Commun. 92*, 883–888.
Jeener, J., Meier, B. H., Bachman, P., & Ernst, R. R. (1979) *J. Chem. Phys. 71*, 4546–4553.
Karplus, M., & McCammon, J. A. (1979) *Nature 277*, 578.
Karplus, M., & McCammon, J. A. (1981) *CRC Crit. Rev. Biochem. 9*, 293–349.
Karplus, M., & McCammon, J. A. (1983) *Annu. Rev. Biochem. 53*, 263–300.
Karplus, M., & Dobson, C. M. (1986) *Methods Enzymol. 131*, 362–389.
Kay, L. E., Torchia, D. A., & Bax, A. (1989a) *Biochemistry 28*, 8972–8979.
Kay, L. E., Marion, D., & Bax, A. (1989b) *J. Magn. Reson. 83*, 72–84.
Keiter, E. A. (1986) Ph.D. Thesis, University of Illinois.
Lakowicz, J. R., & Weber, G. (1973) *Biochemistry 12*, 4171–4179.
Lakowicz, J. R., & Weber, G. (1980) *Biophys. J. 32*, 591–601.
Levitt, M. (1983) *J. Mol. Biol. 168*, 621–657.
Levitt, M., Sander, C., & Stern, P. S. (1985) *J. Mol. Biol. 181*, 423–447.
Levy, R. M., & Szabo, A. (1982) *J. Am. Chem. Soc. 104*, 2073–2076.
Lipari, G., & Szabo, A. (1980) *Biophys. J. 30*, 489–506.
Lipari, G., & Szabo, A. (1981) *J. Chem. Phys. 75*, 2971–2976.
Lipari, G., & Szabo, A. (1982a) *J. Am. Chem. Soc. 104*, 4546–4559.
Lipari, G., & Szabo, A. (1982b) *J. Am. Chem. Soc. 104*, 4559–4570.
Lipari, G., Szabo, A., & Levy, R. M. (1982) *Nature 300*, 197–198.
Llinas, M., & Wüthrich, K. (1978) *Biochim. Biophys. Acta 532*, 29–40.
London, R. E. (1980) in *Magnetic Resonance in Biology* (Cohen, J. S., Ed.) Vol. 1, pp 1–69, Wiley, New York.
London, R. E., & Avitabile, J. (1978) *J. Am. Chem. Soc. 100*, 7159–7165.
Macura, S., Huang, Y., Suter, D., & Ernst, R. R. (1981) *J. Magn. Reson. 43*, 259–281.
Marion, D., & Wüthrich, K. (1983) *Biochem. Biophys. Res. Commun. 113*, 967–974.
Marion, D., Ikura, M., Tschudin, R., & Bax, A. (1989) *J. Magn. Reson. 85*, 393–399.
McCain, D. C., & Markley, J. L. (1987) *J. Magn. Reson. 73*, 244–251.
McCain, D. C., Ulrich, E. L., & Markley, J. L. (1988) *J. Magn. Reson. 80*, 296–305.
McConnell, H. M. (1958) *J. Chem. Phys. 28*, 430–434.
Merola, F., Rigler, R., Holmgren, A., & Brochon, J.-C. (1989) *Biochemistry 28*, 3383–3398.
Moore, M. A. S. (1989) *Immunol. Res. 8*, 165–175.
Nadler, W., & Schulten, K. (1984) *Proc. Natl. Acad. Sci. U.S.A. 81*, 5719–5723.
Nirmala, N. R., & Wagner, G. (1988) *J. Am. Chem. Soc. 110*, 7557–7558.
Nirmala, N. R., & Wagner, G. (1989) *J. Magn. Reson. 82*, 659–661.
Norton, R. E., Clouse, A. O., Addleman, R., & Allerhand, A. (1977) *J. Am. Chem. Soc. 99*, 79–83.
Oppenheim, J. J., Kovacs, E. J., Matsushima, K., & Durum, S. K. (1986) *Immunol. Today 7*, 45–56.
Parak, F., Frolov, E. N., Mössbauer, R. L., & Goldanskii, V. I. (1981) *J. Mol. Biol. 145*, 825–833.
Parak, F., Knapp, E. W., & Kucheida, D. (1982) *J. Mol. Biol. 161*, 177–194.
Parak, F., & Knapp, E. W. (1984) *Proc. Natl. Acad. Sci. U.S.A. 81*, 7088–7092.
Post, C. B., Dobson, C. M., & Karplus, M. (1989) *Proteins: Struct., Funct., Genet. 5*, 337–354.
Powell, M. J. D. (1965) *Comput. J. 7*, 303–307.
Priestle, J. P., Schär, H.-P., & Grütter, M. G. (1989) *Proc. Natl. Acad. Sci. U.S.A. 86*, 9667–9671.
Richarz, R., Nagayama, K., & Wüthrich, K. (1980) *Biochemistry 19*, 5189–5196.
Ringe, D., & Petsko, G. (1985) *Prog. Biophys. Mol. Biol. 45*, 197–235.
Schiksnis, R. A., Bogusky, M. J., Tsang, P., & Opella, S. J. (1987) *Biochemistry 26*, 1373–1381.
Shaka, A. J., Barker, P. B., & Freeman, R. (1985) *J. Magn. Reson. 64*, 547–552.
Smith, G. M., Yu, P. L., & Domingues, D. J. (1987) *Biochemistry 26*, 2202–2207.
Sternberg, M. J. E., Grace, D. E. P., & Philips, D. C. (1979) *J. Mol. Biol. 130*, 231–253.
Tainer, J. A., Getzoff, E., Alexander, J., Houghton, R. A., Olson, A. J., Lerner, R. A., & Hendrickson, W. A. (1984) *Nature 312*, 127–134.
Wagner, G. (1983) *Q. Rev. Biophys. 16*, 1–57.
Westhof, E., Altschu, D., Moras, D., Bloomer, A. C., Mondragon, A., Klug, A., & van Regenmortel, M. H. V. (1984) *Nature 311*, 123–126.
Williams, R. J. P. (1989) *Eur. J. Biochem. 183*, 479–497.
Willis, B. T. M., & Pryor, A. W. (1975) *Thermal Vibrations in Crystallography*, Cambridge University Press, Cambridge, England.
Wingfield, P. T., Payton, M., Tavernier, J., Barnes, M., Shaw, A., Rose, K., Somona, M. G., Demaczuk, S., Williamson, K., & Dayer, J.-M. (1986) *Eur. J. Biochem. 160*, 491–497.
Wittebort, R. J., & Szabo, A. (1978) *J. Chem. Phys. 69*, 1722–1736.
Wittebort, R. J., Szabo, A., & Gurnd, F. R. N. (1980) *J. Am. Chem. Soc. 102*, 5723–5728.
Wodak, S. J., de Crombrugghe, M., & Janin, J. (1987) *Prog. Biophys. Mol. Biol. 49*, 29–63.
Woodward, C. K., & Hilton, B. D. (1979) *Annu. Rev. Biophys. Bioeng. 8*, 99–127.

Jansonius, J. N., Eichele, G., Ford, G. C., Picot, D., Thaller, C., & Vincent, M. G. (1985) in *Transaminases* (Christen, P., & Metzler, D. E., Eds.) pp 110–137, Wiley, New York.
Jencks, W. P. (1975) *Adv. Enzymol. 43*, 219–410.
Jenkins, W. T., & Sizer, I. W. (1957) *J. Am. Chem. Soc. 79*, 2655–2656.
Jenkins, W. T., Yphantis, D. A., & Sizer, I. W. (1959) *J. Biol. Chem. 234*, 51–57.
Julin, D. A., & Kirsch, J. F. (1989) *Biochemistry 28*, 3825–3833.
Kiick, D. M., & Cook, P. F. (1983) *Biochemistry 22*, 375–382.
Kirsch, J. F., & Toney, M. D. (1990) *Ann. N.Y. Acad. Sci. 585*, 48–57.
Kirsch, J. F., Eichele, G., Ford, G. C., Vincent, M. G., Jansonius, J. N., Gehring, H., & Christen, P. (1984) *J. Mol. Biol. 74*, 497–525.
Kirsch, J. R., Finlayson, W. L., Toney, M. D., & Cronin, C. N. (1987) in *Proceedings of the 7th International Congress on Chemical and Biological Aspects of Vitamin B_6 Catalysis* (Korpela, T., & Christen, P., Eds.) pp 59–67, Birkhauser-Verlag, Basel.
Kirsch, J. F., Toney, M. D., & Goldberg, J. M. (1990) in *Protein and Pharmaceutical Engineering* (Craik, C. S., Fletterick, R., Matthews, C. R., & Wells, J., Eds.) pp 105–118, Wiley-Liss, New York.
Kuramitsu, S., Okuno, S., Ogawa, T., Ogawa, H., & Kagamiyama, H. (1985) *J. Biochem. (Tokyo) 97*, 1259–1262.
Malcolm, B. A., & Kirsch, J. F. (1985) *Biochem. Biophys. Res. Commun. 132*, 915–921.
Morino, Y., Shimada, K., & Kagamiyama, H. (1990) *Ann. N.Y. Acad. Sci. 585*, 32–47.
Polyanovskii, O. L. (1963) *Biochemistry (Engl. Transl.) 28*, 751–754.
Scopes, R. K. (1982) *Protein Purification*, pp 241–242, Springer-Verlag, New York.
Smith, D. L., Ringe, D., Finlayson, W. L., & Kirsch, J. F. (1986) *J. Mol. Biol. 191*, 301–302.
Smith, D. L., Almo, S. C., Toney, M. D., & Ringe, D. (1989) *Biochemistry 28*, 8161–8167.
Sober, H. A., Ed. (1968) *CRC Handbook of Biochemistry*, pp J222–J235, Chemical Rubber Co., Cleveland, OH.
Toney, M. D., & Kirsch, J. F. (1987) *J. Biol. Chem. 262*, 12403–12405.
Toney, M. D., & Kirsch, J. F. (1989) *Science 243*, 1485–1488.
Velick, S. F., & Vavra, J. (1962) *J. Biol. Chem. 237*, 2109–2122.
Yagi, T., Kagamiyama, H., Motosugi, K., Nozaki, M., & Soda, K. (1979) *FEBS Lett. 100*, 81–84.
Ziak, M., Jaussi, R., Gehring, H., & Christen, P. (1990) *Eur. J. Biochem. 187*, 329–333.

CORRECTIONS

Absorption and Fluorescence Spectroscopic Studies of the Ca^{2+}-Dependent Lipid Binding Protein p36: The Annexin Repeat as the Ca^{2+} Binding Site, by Gerard Marriott,* William R. Kirk, Nils Johnsson, and Klaus Weber, Volume 29, Number 30, July 31, 1990, pages 7004–7011.

Page 7005. In column 2, line 16 under Results, ^1L_a should read ^1L_b.

Page 7006. In column 1, line 6, and column 2, line 4, ^1L_a should read ^1L_b.

Page 7008. In the caption to Figure 7, lines 1 and 2, spectra of human and chicken p36 should read spectra of human p36.

Page 7009. In column 1, lines 26 and 30, ^1L_a should read ^1L_b.

Analysis of the Backbone Dynamics of Interleukin-1β Using Two-Dimensional Inverse Detected Heteronuclear ^{15}N–^1H NMR Spectroscopy, by G. Marius Clore,* Paul C. Driscoll, Paul T. Wingfield, and Angela M. Gronenborn*, Volume 29, Number 32, August 14, 1990, pages 7387–7401.

Page 7394. Equations 13 and 14 should read as follows:

$$J(\omega_i) = S_f^2 S_s^2 \tau_R/(1 + \omega_i^2 \tau_R^2) + (1 - S_f^2)\tau_f'/(1 + \omega_i^2 \tau_f'^2) + S_f^2(1 - S_s^2)\tau_s'/(1 + \omega_i^2 \tau_s'^2) \quad (13)$$

$$J(\omega_i) = S_f^2 S_s^2 \tau_R/(1 + \omega_i^2 \tau_R^2) + S_f^2(1 - S_s^2)\tau_s'/(1 + \omega_i^2 \tau_s'^2) \quad (14)$$

All calculations presented in the paper were carried out with the correct versions of eqs 13 and 14.